Hindawi
Structural Control and Health Monitoring
Volume 2023, Article ID 9271433, 25 pages
https://doi.org/10.1155/2023/9271433

Research Article

A Nonparametric Bayesian Approach for Bridge Reliability Assessment Using Structural Health Monitoring Data

Ran Chen[1] **and Yi-Qing Ni**[2]

[1]*School of Civil Engineering and Transportation, South China University of Technology, Tianhe, Guangzhou, China*
[2]*Department of Civil and Environmental Engineering, The Hong Kong Polytechnic University, Hung Hom, Kowloon, Hong Kong SAR, China*

Correspondence should be addressed to Yi-Qing Ni; ceyqni@polyu.edu.hk

Received 31 October 2022; Revised 11 March 2023; Accepted 31 March 2023; Published 8 May 2023

Academic Editor: Francesc Pozo

Integrating structural health monitoring (SHM) data into reliability assessment has increasingly been practiced in the condition evaluation of in-service bridges over the past decade. The selection of probability distribution models for load- and resistance-related random variables is a prerequisite for monitoring-based reliability assessment. However, the underlying probabilistic assumptions of the used models could be restrictive and unverifiable especially when dealing with real-world heterogeneous monitoring data, weakening the confidence on the estimated reliability index. This study aims to develop a nonparametric Bayesian model with the Dirichlet process prior for bridge reliability assessment, where the model order constraint can be released such that the complexity of the model adapts to the observed data. Reliability analysis via the nonparametric Bayesian model allows the aleatory uncertainty and the epistemic uncertainty arising from monitoring data to be concurrently accounted for in the formulated reliability index. A numerical example is presented to verify the effectiveness of the nonparametric Bayesian model for dealing with multimodal data. The feasibility of the proposed approach for reliability assessment is then demonstrated with one-year strain monitoring data acquired from a large-scale bridge instrumented with the SHM system.

1. Introduction

Exposed to aggressive environmental conditions and confronted with ever-growing traffic demands, large-scale bridges suffer from unavoidable deterioration over their life cycle. Health condition of in-service bridges is no doubt a main concern to the stakeholders and the professionals, and methods for bridge condition assessment have been widely studied over the past three decades [1–7]. Conventional practice involved in bridge condition assessment includes but not limited to visual inspection, nondestructive testing, controlled load testing, and instrumentation with the structural health monitoring (SHM) system. Benefitting from the rapid advances in sensing, data acquisition, data processing, data management, and computing technologies, the deployment of SHM systems on bridge structures is becoming popular across countries around the world [8–13]. With the use of multiple types of sensors permanently deployed on bridges, the on-structure long-term SHM systems enable to collect measurement data automatically and continuously about the structural responses, external loadings, and environmental effects for in-service bridges. In this connection, instrumentation with the on-line SHM system plays a key role in bridge inspection that allows neither access to the bridge nor interruption of traffic service. SHM-enriched bridge condition assessment is deemed to be an objective approach to raise judicious decisions for inspection and repair, leading to condition-based preventive maintenance of in-service bridges that facilitates the optimal use of limited resources.

In recognition of the existence of substantial uncertainties that affect structural condition assessment, reliability-based methods have been developed for bridge assessment in component and/or system levels in view of

their ability to address randomness in load- and resistance-related variables [1, 14]. Apparently, the inclusion of site-specific long-term monitoring data helps to alleviate the extent of uncertainty in probability models associated with load and resistance, leading to higher confidence in the estimated reliability index [3, 4, 15–17]. The selection of probability distribution models for load- and resistance-related random variables is a fundamental requirement in the execution of monitoring-based reliability assessment. It is common to employ standard distribution models such as normal, log-normal, Weibull, and Gumbel to depict the statistical characteristics of random variables involved in the assessment. However, the standard distribution models can barely capture complicated distributional features such as skewness, asymmetry, heavy-tail, or multimodality encountered in real-world measurement data. In reality, in-service bridges are concurrently subjected to multiple types of loadings including highway traffic, railway traffic, monsoon, typhoon, ambient temperature, and their combinations, resulting in heterogeneous structural responses with multimodal distribution properties [5, 16–19]. The use of conventional unimodal distribution models to represent the multimodal structural responses observed may cause considerable bias in model estimation.

To address the above issue, the finite mixture distribution models [20, 21], which comprise multiple weighted component densities, have been put forward to interpret real datasets with heterogeneity. Ni et al. [5, 22] proposed a model of mixture of multivariate distributions to formulate the SHM-derived stress spectrum for fatigue reliability assessment of steel bridges. Xia et al. [18] conducted reliability assessment for a large-scale bridge where the Weibull mixture distribution in conjunction with the expectation maximization algorithm was applied to characterize the monitored stress responses. Obrien et al. [23] adopted bimodal and trimodal normal distribution models to, respectively, describe the data of gross vehicle weight and axle spacing recorded by weigh-in-motion stations. Li et al. [24] employed the Gaussian mixture model for pattern modelling of the cable tension ratio with intent to assess the condition of stay cables. Ye et al. [25] developed a genetic algorithm-based finite mixture modelling approach to construct the joint distribution of wind speed and wind direction measured from a bridge SHM system. In the aforementioned studies, the mixture parameters (component parameters and mixing weights) were estimated based on the classical frequentist probability theory, with the use of inference techniques such as the expectation maximization algorithm, the hybrid estimation method, and the genetic algorithm. In this regard, only optimal point estimates of the unknown mixture parameters were available, whereas uncertainties inherent in the mixture parameters arising from variability and error in the observed data as well as due to model imperfection were neglected in the frequentist approach. The Bayesian probability theory provides a promising framework to statistical inference on observed data, in particular the ability to interpret uncertainties in parameter and model estimations [26]. An increasing amount of research has been devoted to applying Bayesian inference techniques for uncertainty quantification of engineering problems, including model updating [27–29], system identification [30–34], vibration-based damage detection [35–39], and reliability analysis [40–44]. Recently, the Bayesian inference on mixture models has been explored in order to further account for the uncertainty in estimation of mixture parameters. Figueiredo et al. [45] presented a Bayesian inference-based mixture distribution approach to clustering structural responses for damage detection of bridges under temperature variability. Ni and Chen [46] proposed a monitoring-based bridge reliability assessment procedure in terms of the Bayesian mixture model.

In the application of parametric mixture models, the number of components, also known as model order, is often required to be specified in advance of the statistical inference, which is equivalent to posing restrictive constraint on the complexity of the model. Over- or under-fitting of the parametric model may arise due to the discrepancy between model complexity and unknown data to be interpreted. Therefore, a challenging issue in parametric modelling is how to determine the optimal model for the data. Although model selection metrics such as Akaike's information criterion, the Bayesian information criterion, and the Bayes factor were used in the previous studies to find the mixture model with optimal number of components, the computational cost is prohibitively high, especially under a multitude of candidate models. The nonparametric Bayesian inference [47–49] paves a novel way to sidestep the optimal model selection problem. Rather than competing multiple candidate models with varying complexities, the nonparametric Bayesian approach is to fit a single model whose complexity can freely adapt to the data. As opposed to parametric models equipped with fixed number of parameters, the nonparametric Bayesian models are built upon an infinite-dimensional parameter space, allowing the complexity of the models to be expandable when more data are observed. The nonparametric Bayesian approach has been applied to address statistical and machine learning tasks, for example, regression, classification, clustering, density estimation, and time series modelling [47, 49], showing favorable modelling capabilities. Recently, the attempts to use the nonparametric Bayesian models for SHM applications were also reported, including health diagnosis under changing environmental conditions [50, 51] and operational modal analysis [52].

A nonparametric Bayesian mixture model-based approach for reliability assessment of in-service bridges using long-term SHM data is put forward in this study, which is an extension of the authors' work on reliability assessment of in-service bridges using long-term SHM data and the parametric Bayesian mixture model [46]. The Dirichlet process prior, a prior over distributions with wide support, is employed for the nonparametric Bayesian inference such that the number of components in the elicited mixture model is itself a random variable depending on the volume of observed data. The inference of the nonparametric Bayesian mixture model in line with monitoring data then simultaneously recovers both the most plausible number of components needed and the most plausible mixture PDF, as

well as their associated uncertainties. In this regard, the nonparametric Bayesian mixture model without model order constraint stands to be an improvement over the parametric counterpart [46]. Through modelling random variables via the nonparametric Bayesian mixture model in reliability analysis, it allows both the intrinsic variability and the statistical modelling uncertainty arising from monitoring data to be accounted for in the elicited reliability index.

This article is organized as follows: Fundamentals of the Dirichlet process and formulation of the nonparametric Bayesian mixture model with the Dirichlet process prior are introduced in Section 2. By marginalizing out the unknown component parameters from the conditional posterior probability distribution, an efficient collapsed Gibbs sampler is explored to iteratively perform the posterior inference on the mixture model, whilst a scale reduction factor-based diagnostic is used to quantitatively examine the convergence of the Gibbs iteration process. Section 3 proposes a bridge reliability assessment procedure in terms of the nonparametric Bayesian mixture model, where the elicited conditional reliability index is successively updatable with accumulatively collected SHM data. A numerical example involving estimation of the multimodal dataset is presented in Section 4 to verify the effectiveness of the nonparametric Bayesian mixture model. A case study by using one-year strain monitoring data acquired from the suspension Tsing Ma Bridge is provided in Section 5 to demonstrate the proposed reliability assessment procedure in compliance with the nonparametric Bayesian model, where monthly evolution of the reliability estimates of the deck cross-section members is derived. Results are also compared with those obtained by the parametric Bayesian approach. Section 6 summarizes key findings of the study and gives concluding remarks.

2. Nonparametric Bayesian Mixture Model

2.1. From Parametric to Nonparametric Models. Before proceeding to the nonparametric Bayesian mixture model, it is instructive to review the parametric finite mixture model (FMM). Let $p(\bullet)$ denote the probability density function (PDF) of a random variable. The parametric FMM is composed of finite number of weighted standard distributions, and the PDF can be parametrically expressed [20, 21] as follows:

$$p(y \mid \boldsymbol{\theta}) = \sum_{k=1}^{K} \omega_k f\left(y \mid \theta_k\right), \tag{1}$$

where $f(\bullet \mid \theta_k)$ is the k th component density parameterized by θ_k; ω_k denotes the mixing weight of the k th component, satisfying $0 \le \omega_k \le 1$ and $\sum_{k=1}^{k} \omega_k = 1$; and $K \in \mathbb{Z}^+$ is the prespecified constant model order. In the Bayesian paradigm, the unknown mixture parameters $\boldsymbol{\theta} = \{\omega_1, \cdots, \omega_K, \theta_1, \cdots, \theta_K\}$ are treated as random variables, whose most plausible estimates and the associated uncertainties can be inferred from the observed data. As can be seen, the model order K of the parametric FMM is restricted, with the Bayesian inference on the mixture parameters $\boldsymbol{\theta}$ being pursued within a fixed and finite-dimensional parameter space. When there is mismatch between the complexity of the model and the amount of data available, the trained model may suffer from over- or underfitting of data.

The nonparametric Bayesian mixture model is a flexible alternative to the parametric counterpart. Now, suppose a sequence of data $\mathbf{y} = \{y_1, \cdots, y_N\}$ is observed and consider a special case that each data point is assigned to a unique component, i.e., K is equal to the number of data points N. When sufficient data points stream in, the nonparametric solution can be viewed as an extension of the parametric FMM by taking K to be a countably infinite integer as follows:

$$p(y \mid \boldsymbol{\theta}) = \sum_{k=1}^{\infty} \omega_k f\left(y \mid \theta_k\right), \tag{2}$$

where $\boldsymbol{\theta}$ encapsulates the entire set of the infinite-dimensional mixture parameters. Equation (2) is referred to as the infinite mixture model (IMM) [53], where K depends on N. Through defining the model over an infinite-dimensional parameter space, it enables the nonparametric Bayesian model to invoke a finite subset of the available mixture parameters in inference, whilst the invoked parameter dimension relies on the observed data set. In other words, it is not necessary to employ as many clusters as the data points; instead, only a finite number of effective components are needed to represent the model. As such, aside from the uncertain mixture parameters, the model order K is admitted to be a random variable that adapts to the size of observed data. Learning the nonparametric Bayesian model from data automatically recovers both the most plausible model order and the most plausible mixture PDF, as well as the associated uncertain bounds.

By expunging the assumption of fixed model order, the nonparametric Bayesian approach affords greater flexibility in data interpretation and data-driven modelling than the parametric counterpart.

2.2. Dirichlet Process Prior. In pursuit of the Bayesian inference of nonparametric models such as the IMM, one needs to first select prior distributions for the infinite-dimensional model parameters $\boldsymbol{\theta}$. Unlike imposing prior distributions on the parameters of the FMM separately, the infinite-dimensional parameter space typically constitutes functions or measures, therefore requiring workable priors over functions or measures other than individual parameters. The Dirichlet process (DP) is an appropriate choice being the prior over distributions, and it is also one of the building blocks in nonparametric Bayesian methods [49]. In this section, fundamental properties of the DP will be outlined, which are essential to formulate the nonparametric Bayesian mixture model.

The DP is a stochastic process whose generated trajectories are probability measures with probability one. Samples from a DP can be interpreted as random probability distributions, and one may loosely view the DP as a distribution over distributions. Formally, a random probability

function G to be distributed according to a DP can be written [54] as follows:

$$G \sim DP(\alpha, G_0), \tag{3}$$

where G_0 is a base measure over the probability space and $\alpha \in \mathbb{R}^+$ is a positive concentration parameter. Roles of G_0 and α playing in a DP are analogous to those of mean and variance in a normal distribution: (1) the base measure G_0 is the expectation of G, i.e., realizations from the DP fall around G_0; and (2) the concentration parameter α reflects the diffusion of G about G_0, i.e., the larger the value of α, the more concentrated the realizations around the mean.

As G is a distribution, a sequence of independent and identically distributed samples $\{\theta_1, \cdots, \theta_N\}$ can be drawn from G itself. The posterior distribution of G conditioned on the observed values of $\{\theta_1, \cdots, \theta_N\}$ is again a DP with an updated concentration parameter and base measure as follows:

$$G \,|\, \theta_1, \cdots, \theta_N \sim DP\left(\alpha + N, \frac{\alpha}{\alpha + N} G_0 + \frac{N}{\alpha + N} \frac{\sum_{i=1}^{N} \delta_{\theta_i}}{N}\right), \tag{4}$$

where δ_{θ_i} is the Dirac measure (a point mass) located at atom θ_i. The posterior base measure is the predictive distribution of θ_{N+1} as follows:

$$\theta_{N+1} \,|\, \theta_1, \cdots, \theta_N \sim \frac{\alpha}{\alpha + N} G_0 + \frac{N}{\alpha + N} \frac{\sum_{i=1}^{N} \delta_{\theta_i}}{N}, \tag{5}$$

where the random G has been marginalized out. Notice that the right-hand side of equation (5) consists of a weighted average over the prior base measure G_0 and the empirical distribution $\sum_{i=1}^{N} \delta_{\theta_i}/N$ of θ. Specifically, the predictive distribution (5) states that if one draws a distribution $G \sim DP(\alpha, G_0)$ and then draws a sequence of samples $\theta_1, \cdots, \theta_N \sim G$, it endows a new sample θ_{N+1} with a positive probability to be relocated at previous draws $\theta_1, \cdots, \theta_N$. Since the value of any draw from G can be repeated by another draw, it further implies that G is a discrete distribution regardless of the smoothness of G_0. In addition, for a long enough sequence of samples from G, multiple θ_i's can share with an identical value, casting in group structures of the sequence of $\{\theta_1, \cdots, \theta_N\}$. The discreteness and clustering properties enable a DP to serve as a nonparametric prior for mixture models.

The clustering property of a DP renders a random partition over the data index set $\{1, \cdots, N\}$. The distribution over the random partitions is called the Chinese restaurant process (CRP) [55] due to a metaphor. Imagine a restaurant with infinitely many tables and a sequence of customers waiting outdoor. The first customer enters and sits on the first table, followed by the second customer who sits in the first table with probability of $1/(1 + \alpha)$, or chooses a new table with probability of $\alpha/(1 + \alpha)$. The generalization of the CRP is that the ith customer either chooses the kth occupied table with probability proportional to the number of customers already sitting there or sits on a new unoccupied table with probability proportional to α. At any time point of this process, the allocation of customers to tables defines a random partition. Let $P(\bullet)$ denote the probability of a random event. Formally, the conditional probability governing the CRP can be expressed as follows: Let $z_i = k$ be the allocation for the ith customer to the kth table. Samples from the CRP can be drawn [48] as follows:

$$P\left(z_i = k \,|\, \mathbf{z}_{-i}\right) = \begin{cases} \dfrac{n_{-i,k}}{\alpha + N - 1}, & \text{if } k \text{ is an occupied table,} \\ \dfrac{\alpha}{\alpha + N - 1}, & \text{if } k \text{ is a new table,} \end{cases} \tag{6}$$

where $\mathbf{z}_{-i}$ are the allocations of $n - 1$ customers excluding the ith customer and $n_{-i,k}$ is the number of customers sitting at the kth table excluding the ith customer. As such, clustering using unbounded mixture models can be characterized by the CRP, where the customers represent the indices associated with observations and tables represent the infinitely many components.

The explicit realization of a DP is attained by the stick-breaking construction [56] as follows:

$$\beta_k \sim \mathscr{B}(1, \alpha), \tag{7a}$$

$$\omega_k = \beta_k \prod_{l=1}^{k-1} (1 - \beta_l), \tag{7b}$$

$$\theta_k^* \sim G_0, \tag{7c}$$

$$G = \sum_{k=1}^{\infty} \omega_k \delta_{\theta_k^*}, \tag{7d}$$

where $\mathscr{B}$ denotes the beta distribution and θ_k^* is the kth unique value of $\{\theta_1, \cdots, \theta_N\}$. Suppose there is a stick of length one, the total probability is represented to be assigned to the atoms. The stick is first cut off with a length of $\beta_1 \sim \mathscr{B}(1, \alpha)$, and a probability mass of $\omega_1 = \beta_1$ is assigned to the first generated atom $\theta_1^* \sim G_0$. Then, the remaining $(1 - \beta_1)$ length of the stick is again cut off with a length of $\beta_2 \sim \mathscr{B}(1, \alpha)$. Meanwhile, a probability mass of $\omega_2 = \beta_2(1 - \beta_1)$ is assigned to the next generated atom $\theta_2^* \sim G_0$. The process continues so that the stick is divided into infinite number of segments with each segment representing weighted point mass. The infinite sum of the weighted point masses constitutes the discrete random distribution G, which is DP-distributed. The stick-breaking construction over $\boldsymbol{\omega} = \{\omega_k\}_{k=1}^{\infty}$ can be conveniently written as $\boldsymbol{\omega} \sim \mathrm{GEM}(\alpha)$.

2.3. Dirichlet Process Gaussian Mixture Model. Since random distributions drawn from a DP are of discreteness without any PDFs, it is inappropriate to employ the DP directly as a prior distribution on the mixture model if the aim is to estimate the underlying PDF of the observed data. A nonparametric solution to this issue is the kernel technique by convolving G with a continuous density function [26] as follows:

$$p(y) = \int \mathscr{K}(y \mid \theta) dG(\theta), \tag{8}$$

where $\mathscr{K}(\bullet \mid \theta)$ is a continuous kernel density function indexed by θ and $G \sim DP(\alpha, G_0)$. If the Gaussian density is adopted as the kernel, the nonparametric density as defined by equation (8) resembles the IMM of equation (2) due to the clustering property of the DP, where y_i's sharing the same value of θ_i are classified as a cluster. The resulted model is referred to as the Dirichlet process Gaussian mixture model (DPGMM). In this study, the base measure G_0 is chosen to be the normal-inverse-chi-square distribution, which is a conjugate prior for the Gaussian kernel, and the atom $\theta_i = \{\mu_i, \sigma_i^2\}$ is the mean and variance of the Gaussian kernel. With the aid of DP's stick-breaking construction, the DPGMM can be explicitly expressed in a sampling form [54] as follows:

$$\boldsymbol{\omega} \sim \mathrm{GEM}(\alpha), \tag{9a}$$

$$z_i \mid \boldsymbol{\omega} \sim \mathrm{Mult}(\boldsymbol{\omega}), \tag{9b}$$

$$\theta_k^* \sim \mathscr{H}\left(\xi_0, \kappa_0, s_0^2, \nu_0\right), \tag{9c}$$

$$y_i \mid z_i, \{\theta_k^*\}_{k=1}^{\infty} \sim \mathscr{N}\left(\theta_{z_i}^*\right), \tag{9d}$$

where $\boldsymbol{\omega}$ are the mixing weights generated by equations (7a)–(7d); z_i is the component indicator of y_i, and it is drawn from a multinomial distribution denoted as Mult; $\mathscr{H}$ is the normal-inverse-chi-square distribution with $\{\xi_0, \kappa_0, s_0^2, \nu_0\}$ being its hyperparameters; and $\theta_k^* = \{\mu_k, \sigma_k^2\}$ is the kth Gaussian parameter drawn from $\mathscr{H}$. A graphical representation of the DPGMM is shown in Figure 1(a). As can be seen, the DPGMM is a mixture model with countably infinite number of components; however, because the mixing weights ω_k's decrease exponentially quickly according to the DP's stick-breaking construction, only a limited number of effective components will be invoked in the DPGMM. The model complexity of the DPGMM can freely accommodate the amount of observed data, which is different from the finite Gaussian mixture model (FGMM) shown in Figure 1(b) that fits data using a fixed number of Gaussian components.

2.4. Posterior Inference Using the Collapsed Gibbs Sampler. Exact inference on DP-based models is computationally intractable since the analytical posterior distributions of the models are often inexistent. In recent years, approximate Bayesian inference algorithms based on the Markov chain Monte Carlo (MCMC) strategy have been developed to numerically pursue the posterior distributions of the models [26]. The logic of the MCMC-based algorithms is to generate a sequence of samples from the approximate distribution and then correct the samples such that the limiting distribution will be close to the target distribution. In this study, the collapsed Gibbs sampler [57], an efficient MCMC-based algorithm, is employed to estimate the posterior PDF of the DPGMM. The procedure of the collapsed Gibbs sampler is summarized in Figure 2. In contrast to the Gibbs sampler applied in the FGMM [46], the collapsed Gibbs sampler enables a higher posterior sampling efficiency to be attained by working in a low-dimensional parameter space through marginalizing out the unknown Gaussian parameter θ_k^* from the conditional posterior probability. To be more specific, the collapsed Gibbs sampler is pursued in a back-to-front way that, in each iteration step, one may temporarily waive the sampling of θ_k^* for each component and instead draw the component indicator z_i for each data item y_i first as shown in the blue box in Figure 2. It is feasible because the conjugate prior used allows θ_k^* to be integrated out and the conditional posterior probability of z_i is analytically available. According to the clustering property of the DP, in each iteration step, the y_i's with the same assignment $z_i = k$ are probabilistically grouped together as the kth cluster and θ_k^* can be directly estimated by the conditional posterior distributions as shown in the green box in Figure 2. Evidently, it is more efficient to draw θ_k^* for y_i's that belong to a same component than to draw θ_i for each y_i in an iteration step.

The conditional posterior distributions of the DPGMM are derived as follows. To elicit the conditional posterior probability of z_i, the CRP representation now serves as the prior probability for z_i since no data have been observed. By applying Bayes' theorem, the conditional posterior probability of z_i after combining the data likelihood is derived as follows:

$$\begin{aligned} P\left(z_i = k \mid \mathbf{z}_{-i}, \mathbf{y}\right) &\propto P\left(z_i = k \mid \mathbf{z}_{-i}\right) p\left(\mathbf{y} \mid z_i = k, \mathbf{z}_{-i}\right) \\ &= P\left(z_i = k \mid \mathbf{z}_{-i}\right) p\left(y_i \mid \mathbf{y}_{-i}, z_i = k, \mathbf{z}_{-i}\right) \\ &\quad p\left(\mathbf{y}_{-i} \mid z_i = k, \mathbf{z}_{-i}\right) \\ &\propto P\left(z_i = k \mid \mathbf{z}_{-i}\right) p\left(y_i \mid \mathbf{y}_{-i,k}\right), \end{aligned} \tag{10}$$

where $\mathbf{y}_{-i}$ is the subset of $\mathbf{y} = \{y_1, \cdots, y_N\}$ without taking account of y_i and $\mathbf{y}_{-i,k}$ is the set of observed data assigned to the kth component without taking account of y_i. The first term on the right-hand side of equation (10) is the prior of z_i which can be readily obtained by equation (6). The second term is the predictive distribution of y_i which has Student's t distribution [58] as follows:

$$\begin{aligned} p\left(y_i \mid \mathbf{y}_{-i,k}\right) &= \int p\left(y_i \mid \theta_k^*\right) p\left(\theta_k^* \mid \mathbf{y}_{-i,k}\right) d\theta \\ \theta &= \mathscr{T}\left(y_i \,\middle|\, \xi_k, \frac{\kappa_k + 1}{\kappa_k \nu_k} s_k^2, \nu_k\right), \end{aligned} \tag{11}$$

in which the hyperparameters are explicitly updated by

$$\xi_k = \frac{\kappa_0 \xi_0 + n_{-i,k} \overline{y}_{-i,k}}{\kappa_0 + n_{-i,k}}, \tag{12a}$$

$$\kappa_k = \kappa_0 + n_{-i,k}, \tag{12b}$$

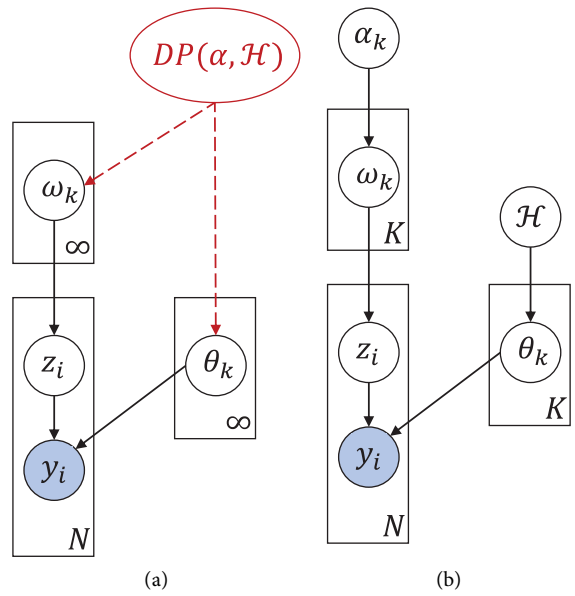

FIGURE 1: Graphical illustrations of the (a) DPGMM and (b) FGMM.

$$s_k^2 = \frac{1}{\nu_0 + n_{-i,k}}\left(\nu_0 s_0^2 + \sum_{h\in k, h\neq i}\left(y_h - \overline{y}_{-i,k}\right)^2 + \frac{\kappa_0 n_{-i,k}}{\kappa_0 + n_{-i,k}}\left(\overline{y}_{-i,k} - \xi_0\right)^2\right), \tag{12c}$$

$$\nu_k = \nu_0 + n_{-i,k}, \tag{12d}$$

where $n_{-i,k}$ and $\overline{y}_{-i,k}$ are the number of samples and the sample mean of $\mathbf{y}_{-i,k}$, respectively. By substituting equations (6) and (11) into equation (10), the conditional posterior probability of z_i is expressed as follows:

$$P\left(z_i = k \,|\, \mathbf{z}_{-i}, \mathbf{y}\right) = \begin{cases} \dfrac{n_{-i,k}}{\alpha + N - 1}\mathcal{T}\left(y_i \,\middle|\, \xi_k, \dfrac{\kappa_k + 1}{\kappa_k \nu_k} s_k^2, \nu_k\right), & \text{for } k \leq K, \\ \dfrac{\alpha}{\alpha + N - 1}\mathcal{T}\left(y_i \,\middle|\, \xi_0, \dfrac{\kappa_0 + 1}{\kappa_0 \nu_0} s_0^2, \nu_0\right), & \text{if } k = K + 1. \end{cases} \tag{13}$$

Notice that the predictive distribution of y_i now has two different expressions: (i) posterior predictive distribution: if $z_i = k\,(k \leq K)$ is an existing component with $\mathbf{y}_{-i,k}$ being the assigned data points, the predictive distribution is Student's t distribution with updated hyperparameters $\{\xi_k, \kappa_k, s_k^2, \nu_k\}$ and then evaluated at y_i; (ii) prior predictive distribution: if $z_i = K + 1$ is a new component given no observations, i.e., $\mathbf{y}_{-i,k} = \varnothing$, the predictive distribution is Student's t distribution with hyperparameters $\{\xi_0, \kappa_0, s_0^2, \nu_0\}$ and then evaluated at y_i. Hence, sampling z_i with equation (11) admits a new component, apart from other existing components, to be created and either to grow up or fade away in a probabilistic manner during the Gibbs iterations. Unlike the FGMM whose model order is a constant, the effective number of components K adopted in the DPGMM is a random variable varying across the posterior samples. In this point, the DPGMM can be viewed as a fully Bayesian approach for mixture modelling in which the unknown mixture parameters and model order are both treated as random variables to be identified from data. Without the need of assuming the model order *a priori*, the DPGMM confers greater data adaptivity and higher error tolerance than the FGMM for interpreting data.

As long as the allocation of data points $\mathbf{z} = \{z_1, \cdots, z_N\}$ is inferred at the current iteration step, the estimation of the Gaussian parameter and the mixing weight for each component can be obtained straightforwardly in a similar way to that of the FGMM [46]. The conditional posterior distribution of the mixing weights $\boldsymbol{\omega}$ obeys to the Dirichlet distribution:

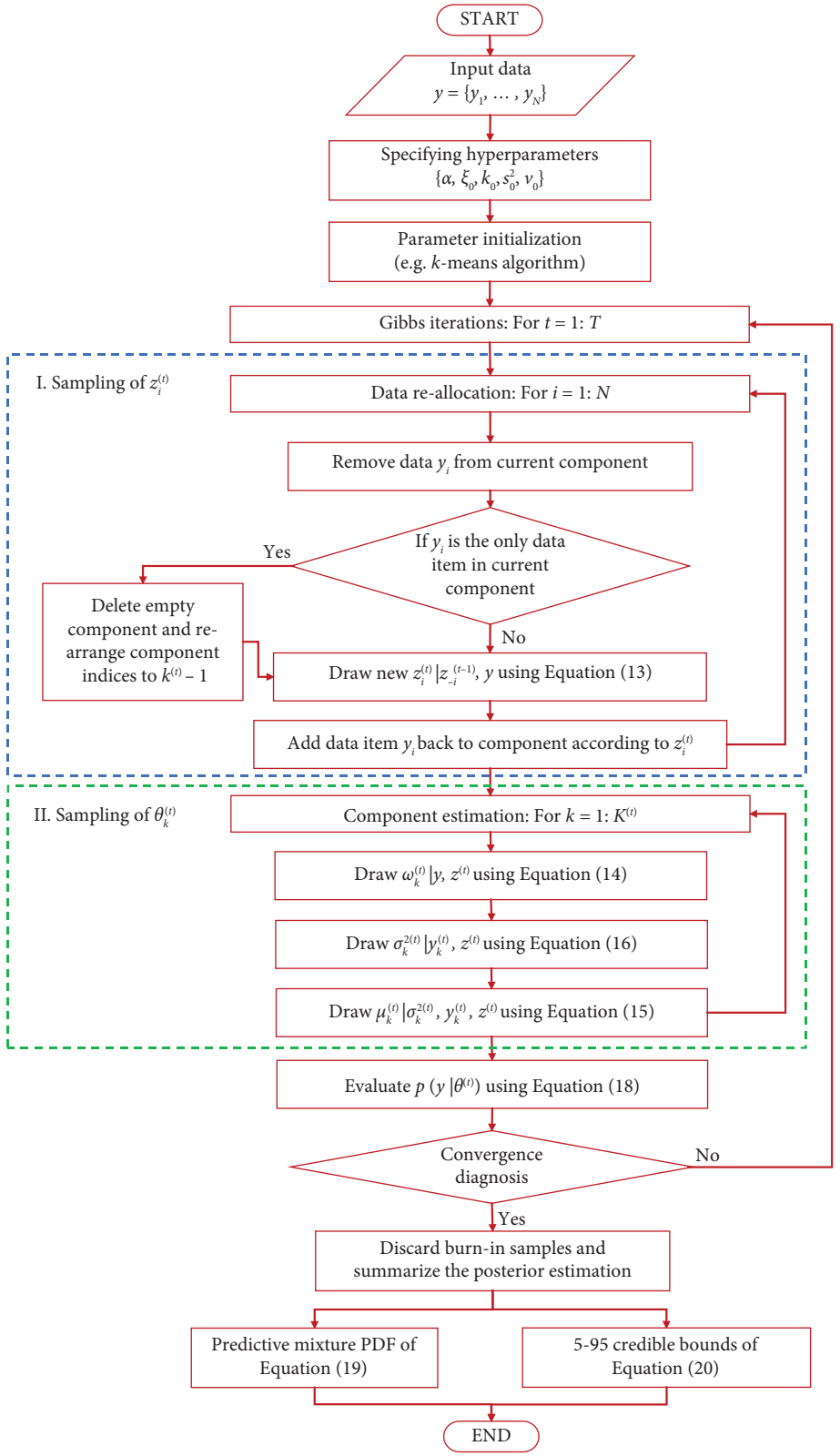

Figure 2: The flowchart of the collapsed Gibbs sampler for the DPGMM.

$$\boldsymbol{\omega} \mid \mathbf{y}, \mathbf{z} \sim Dir\left(n_1, \cdots, n_K\right). \tag{14}$$

The conditional posterior distribution of μ_k given σ_k^2 is the Gaussian density:

$$\mu_k \mid \sigma_k^2, \mathbf{y}_k, \mathbf{z} \sim \mathcal{N}\left(\xi_k, \sigma_k^2/\kappa_k\right), \tag{15}$$

and the marginal posterior distribution of σ_k^2 is the scaled inverse-chi-square density:

$$\sigma_k^2 \mid \mathbf{y}_k, \mathbf{z} \sim InvC\left(\nu_k, s_k^2\right), \tag{16}$$

in which the hyperparameters are explicitly updated by

$$\xi_k = \frac{\kappa_0 \xi_0 + n_k \overline{y}_k}{\kappa_0 + n_k}, \tag{17a}$$

$$\kappa_k = \kappa_0 + n_k, \tag{17b}$$

$$s_k^2 = \frac{1}{\nu_0 + n_k}\left(\nu_0 s_0^2 + \sum_{i \in k}\left(y_i - \overline{y}_k\right)^2 + \frac{\kappa_0 n_k}{\kappa_0 + n_k}\left(\overline{y}_k - \xi_0\right)^2\right), \tag{17c}$$

$$\nu_k = \nu_0 + n_k, \tag{17d}$$

where $\mathbf{y}_k$ is the set of observed data assigned to the kth component; and n_k and $\overline{y}_k$ are the number of samples and the sample mean of $\mathbf{y}_k$, respectively. Notice that equations (17a)–(17d) resemble equations (12a)–(12d) except that the data point y_i is not accounted for in the latter.

Posterior inference with the collapsed Gibbs sampler can be performed once the conditional posterior distributions are accessible. As illustrated in Figure 2, for the tth iteration step ($t = 1, \cdots, T$), the sampler first draws allocation $z_i^{(t)}$ for each data item y_i ($i = 1{:}\ N$) successively with conditional parameters $\mathbf{z}_{-i}^{(t-1)}$ from the previous iteration step $(t-1)$, where a new component may be generated and an empty component without data should be deleted. Then, it draws $\omega_k^{(t)}$, $\mu_k^{(t)}$, and $\sigma_k^{2(t)}$ ($k = 1{:}\ K$) conditioned on the updated data assignment $\mathbf{z}^{(t)}$. The process iterates to produce sequences of posterior model parameters. Since parameter dimension changes across the Gibbs iteration, summarizing the posterior distributions of individual model parameters of the DPGMM is unattainable. In this study, the mixture PDF samples based on the estimated parameters at each Gibbs iteration step are formulated to represent the posterior inference results as follows:

$$p\left(y \mid \boldsymbol{\theta}^{(t)}\right) = \sum_{k=1}^{K^{(t)}} \omega_k^{(t)} \mathcal{N}\left(y \mid \mu_k^{(t)}, \sigma_k^{2(t)}\right), \tag{18}$$

where $\boldsymbol{\theta}^{(t)} = \left\{\boldsymbol{\omega}^{(t)}, \boldsymbol{\mu}^{(t)}, \boldsymbol{\Sigma}^{(t)}, K^{(t)}\right\}$ now encapsulates the estimated model parameters at the t th iteration.

At the beginning of the Gibbs run, the generated PDF samples are far from the true posterior PDF. After discarding a certain number of early draws, referred to as burn-in samples B, the remaining $G = T - B$ samples are deemed as the posterior mixture PDF samples. The Bayesian estimation of the DPGMM is summarized in terms of the generated posterior mixture PDF samples. The predictive mixture PDF is defined as the pointwise mean function of the posterior mixture PDF samples:

$$\widehat{p}(y) = G^{-1} \sum_{g=1}^{G} p\left(y \mid \boldsymbol{\theta}^{(g)}\right). \tag{19}$$

This is a nonparametric density estimation averaging over the trans-dimensional parameter space, which represents the most plausible mixture PDF given the observed data. Meanwhile, the variability of posterior mixture PDF samples reflects the effect of model order and parametric uncertainties (modelling uncertainties) arising from interpreting the observed data with the DPGMM. By measuring the upper and lower credible bounds of the pointwise density, it enables the modelling uncertainties to be explicitly quantified. Let $P = \left\{p(y^* \mid \boldsymbol{\theta}^{(1)}), \cdots, p(y^* \mid \boldsymbol{\theta}^{(G)})\right\}$ denote a set of random density values evaluated at y^* using equation (18). The 5–95 credible bounds of the posterior PDF at y^* can be formulated as follows:

$$\left[P_{0.05}, P_{0.95}\right]. \tag{20}$$

2.5. Quantitative Convergence Diagnosis. Convergence monitoring is important in performing MCMC-based inference techniques because only the generated samples after convergence can be used to represent the true posterior distribution. Convergence diagnosis strategies based on quantitative criteria are generally preferable in that they provide the exact number of iterations needed to attain convergence, thereby avoiding conservative estimates of the burn-in period B and the total number of iterations T.

A scale reduction factor-based diagnosis method [59] is adopted here to quantitatively assess the convergence of the collapsed Gibbs sampler. In this method, the log likelihood values ϕ of the generated mixture PDF samples, being a coherent statistic metric throughout the iterations, are first formulated as follows:

$$\phi^{(t)} = -2\ln\left(p\left(\mathbf{y} \mid \boldsymbol{\theta}^{(t)}\right)\right), \tag{21}$$

where $p(\mathbf{y} \mid \boldsymbol{\theta}^{(t)})$ is evaluated by equation (18) given the observed data $\mathbf{y}$. Then, multiple chains of ϕ can be produced simultaneously via running the collapsed Gibbs sampler from different starting points. By both splitting the sequences of ϕ between chains and between models (generated PDF samples with different K), several types of estimates of variance for ϕ can be constructed as given in Appendix, including the total variance V, the within-chain variance W_c, the within-model variance W_m, the variance within both chains and models $W_m W_c$, the between-model variance B_m, and the within-chain variance split between and averaged over models $B_m W_c$. After sufficient iterations, if the Gibbs iterations are converged, then both V and W_c should well approximate the true variance, both W_m and $W_m W_c$ should well approximate the within-model variance, and both B_m and $B_m W_c$ should well approximate the between-model

variance. Here, the between-model variance refers to the variance of ϕ with respect to the generated PDFs with different K, while the within-model variance refers to the variance of ϕ with respect to the generated PDFs with identical K. Hence, the scale reduction factors of the true variance, the within-model variance, and the between-model variance are formulated as follows:

$$R_T = \sqrt{\frac{T-1}{T} + \frac{V}{TW_c}},$$
$$R_W = \sqrt{\frac{T-1}{T} + \frac{W_m}{TW_mW_c}}, \tag{22}$$
$$R_B = \sqrt{\frac{T-1}{T} + \frac{B_m}{TB_mW_c}}.$$

Evidently, the values of all scale reduction factors will reach one as the iteration goes. In the present study, convergence monitoring is performed by simultaneously generating two chains for ϕ and the convergence is guaranteed when all scale reduction factors satisfy $|R-1| < 10^{-3}$.

3. Reliability Assessment Using the Nonparametric Bayesian Mixture Model

3.1. Formulation of the Conditional Reliability Index. The proposed nonparametric Bayesian model can serve as the statistical descriptive models for reliability assessment to further account for the modelling uncertainties arising from the structural resistance and load effect characterization using monitoring data. Suppose R and S are the structural resistance and the load effect with $\boldsymbol{\theta}_R$ and $\boldsymbol{\theta}_S$ being the associated uncertain model parameters, respectively. The limit state function can be defined as follows:

$$h(\mathbf{X}, \boldsymbol{\Theta}) = R(\boldsymbol{\theta}_R) - S(\boldsymbol{\theta}_S), \tag{23}$$

where $\mathbf{X} = \{R, S\}$ is the set of the basic random variables and $\boldsymbol{\Theta} = \{\boldsymbol{\theta}_R, \boldsymbol{\theta}_S\}$ is the set of uncertain model parameters. Here, $h = 0$ denotes the limit state, while $h < 0$ denotes the failure state. Without loss of generality, the failure probability estimate $\widehat{P}_f$ involving the uncertain model parameters $\boldsymbol{\Theta}$ can be defined [14, 42] as follows:

$$\widehat{P}_f = P(h(\mathbf{X}, \boldsymbol{\Theta}) < 0) = \int_{h<0} \int p_{\mathbf{X}}(\mathbf{x} \mid \boldsymbol{\Theta}) p(\boldsymbol{\Theta} \mid \mathscr{D}) \mathrm{d}\boldsymbol{\Theta}\, \mathrm{d}\mathbf{x}, \tag{24}$$

where $p_{\mathbf{X}}(\mathbf{x} \mid \boldsymbol{\Theta})$ is the joint PDF of $\mathbf{X}$ and $p(\boldsymbol{\Theta} \mid \mathscr{D})$ is the joint posterior PDF of $\boldsymbol{\Theta}$ given the monitoring/test data $\mathscr{D}$. If the posterior PDF $p(\boldsymbol{\Theta} \mid \mathscr{D})$ is sought by an MCMC algorithm, $\widehat{P}_f$ can be efficiently estimated by the Monte Carlo method as follows:

$$\widehat{P}_f = G^{-1} \sum_{g=1}^{G} P_f\left(\boldsymbol{\Theta}^{(g)}\right) = G^{-1} \sum_{g=1}^{G} \int_{h<0} p_{\mathbf{X}}\left(\mathbf{x} \mid \boldsymbol{\Theta}^{(g)}\right) \mathrm{d}\mathbf{x}, \tag{25}$$

where $P_f(\boldsymbol{\Theta}) = \int_{h<0} p_{\mathbf{X}}(\mathbf{x} \mid \boldsymbol{\Theta}) \mathrm{d}\mathbf{x}$ is termed the conditional failure probability. With the inferred posterior samples of $\boldsymbol{\Theta}$, the samples of $P_f(\boldsymbol{\Theta})$ can be readily obtained through well-established reliability computational tools, such as the first-order reliability method (FORM), the second-order reliability method (SORM), and the importance sampling method (ISM) [42]. Equation (25) offers a general solution to the evaluation of failure probability involving uncertain model parameters.

In general, the resistance R and the load effect S can be regarded as mutually independent random variables, i.e., $p_{\mathbf{X}}(\mathbf{x} \mid \boldsymbol{\Theta}) = p_R(r \mid \boldsymbol{\theta}_R) p_S(s \mid \boldsymbol{\theta}_S)$, whilst R can be adequately expressed by a unimodal distribution model. When the load effect S is described with the nonparametric Bayesian mixture model elicited from monitoring data, the samples of $P_f(\boldsymbol{\Theta})$ can be obtained as follows:

$$P_f\left(\boldsymbol{\Theta}^{(g)}\right) = \sum_{k=1}^{K^{(g)}} \boldsymbol{\omega}_{S_k}^{(g)} \int_{h_k<0} p_R\left(r \mid \boldsymbol{\theta}_R^{(g)}\right) p_{S_k}\left(s \mid \boldsymbol{\theta}_{S_k}^{(g)}\right) dr\, ds, \tag{26}$$

where S_k denotes the kth component of the multiload effect; $p_{S_k}(s \mid \boldsymbol{\theta}_{S_k})$ and $\boldsymbol{\omega}_{S_k}$ are the component density and the mixing weight associated with the kth component, respectively; and $\cup_{k=1}^{K^{(g)}} h_k = h$ is the failure domain conditioned on $\boldsymbol{\Theta}^{(g)}$. Equation (26) can be approximated by FORM provided that R and S_k conform to the Gaussian distribution:

$$P_f\left(\boldsymbol{\Theta}^{(g)}\right) \approx \sum_{k=1}^{K^{(g)}} \omega_{S_k}^{(g)} \Phi\left(-\beta_k\left(\boldsymbol{\theta}_R^{(g)}, \boldsymbol{\theta}_{S_k}^{(g)}\right)\right), \tag{27}$$

where $\beta_k(\boldsymbol{\theta}_R, \boldsymbol{\theta}_{S_k}) = (\mu_R - \mu_{S_k}) / (\sigma_R^2 + \sigma_{S_k}^2)^{1/2}$ is the reliability estimate associated with the kth component of load effect conditioned on $\boldsymbol{\theta}_R$ and $\boldsymbol{\theta}_{S_k}$. It follows that the samples of $\beta(\boldsymbol{\Theta})$, termed as the conditional reliability index, can be obtained by

$$\beta\left(\boldsymbol{\Theta}^{(g)}\right) = -\Phi^{-1}\left(P_f\left(\boldsymbol{\Theta}^{(g)}\right)\right), \tag{28}$$

where Φ^{-1} is the inverse cumulative probability density of the standard normal distribution. Equation (28) unveils that the sample value of the conditional reliability index $\beta(\boldsymbol{\Theta})$ is a function with respect to the uncertain model parameters $\boldsymbol{\Theta}$, leading $\beta(\boldsymbol{\Theta})$ itself to be a random variable due to the nature of uncertainty of $\boldsymbol{\Theta}$. In this regard, aside from the intrinsic variability of resistance and load effect, the uncertainties stemming from statistical modelling and measurement error of monitoring data can also have influence on reliability assessment. Hence, a reliability index estimate $\widehat{\beta}$ considering both aleatory uncertainty and epistemic uncertainty can be attained as the sample mean of $\beta(\boldsymbol{\Theta})$ as follows:

$$\widehat{\beta} = \mu_\beta = G^{-1}\sum_{g=1}^{G}\beta\left(\boldsymbol{\Theta}^{(g)}\right). \tag{29}$$

The sample standard deviation of $\beta(\boldsymbol{\Theta})$ quantifies the variation about the reliability index estimate as follows:

$$\sigma_\beta = \sqrt{\frac{\sum_{g=1}^{G}\left(\beta\left(\boldsymbol{\Theta}^{(g)}\right) - \mu_\beta\right)^2}{G-1}}. \tag{30}$$

By virtue of the nonparametric Bayesian method, multiple types of uncertainties in reliability analysis can be effectively treated, making their effects on the reliability estimate be explicitly quantified.

3.2. Bayesian Updating of Reliability Estimate. With successively acquired SHM data, the conditional reliability estimate, which is a random variable, can be regularly updated based on Bayes' theorem to enable an evolutionary structural condition assessment over the concerned monitoring period. The notation β is used instead of $\beta(\boldsymbol{\Theta})$ hereafter for brevity.

In the Bayesian probability theory, assume that the conditional reliability index β conforms to the Gaussian distribution with uncertain parameters $\theta_\beta = \left\{\mu_\beta, \sigma_\beta^2\right\}$. Suppose the reliability estimate for the mth monitoring interval is $\beta^m \sim \mathcal{N}(\beta \mid \theta_\beta^m)$ with the dataset $\mathcal{D}^m$. As the monitoring data accumulate, when the dataset $\mathcal{D}^{m+1}$ in relation to the $(m+1)$ th monitoring interval is available, the samples of β^{m+1} can be obtained using equation (28). However, the conditional reliability index β^{m+1} solely inferred from the dataset $\mathcal{D}^{m+1}$ is potentially biased to portray the current structural condition in that the statistical information of the earlier reliability index β^m has been ignored. To overcome this weakness, the posterior distribution of θ_β^{m+1} is first sought by applying Bayes' theorem:

$$p\left(\theta_\beta^{m+1} \mid \beta^{m+1}\right) \propto p\left(\beta^{m+1} \mid \theta_\beta^m\right) p\left(\theta_\beta^m\right), \tag{31}$$

where $p(\theta_\beta^m)$ is the prior distribution of θ_β for the $(m+1)$ th monitoring interval and it is also the posterior distribution of θ_β for the m th monitoring interval. Updating of the reliability estimate β is achieved by evaluating the posterior predictive distribution as follows:

$$p\left(\widetilde{\beta}^{m+1} \mid \beta^{m+1}\right) = \int p\left(\widetilde{\beta}^{m+1} \mid \theta_\beta^{m+1}, \beta^{m+1}\right) p\left(\theta_\beta^{m+1} \mid \beta^{m+1}\right) \mathrm{d}\theta_\beta^{m+1}, \tag{32}$$

where $\widetilde{\beta}^{m+1}$ is termed the predictive reliability index in relation to the $(m+1)$ th monitoring interval. It is found that $\widetilde{\beta}^{m+1}$ provides more comprehensive information than β^{m+1} in which the former incorporates the historical structural condition knowledge. When the monitoring data are cumulatively available, the Bayesian updating scheme can be successively executed to assess the evolutionary structural condition. Note that equation (32) can be solved analytically if the conjugate prior of θ_β is employed [26].

4. Numerical Example

The nonparametric Bayesian modelling approach, including the DPGMM, the collapsed Gibbs sampler, and the scale reduction factor-based convergence diagnosis method as presented in Section 2, is applied to a trimodal dataset to verify the effectiveness for modelling heterogeneous data. The trimodal dataset with a sample size of 2000 is generated according to the following mixture distribution:

$$0.6\mathcal{N}(1, 0.2) + 0.2\mathcal{N}(5, 2) + 0.2\mathcal{N}(10, 1). \tag{33}$$

Figure 3(a) shows the histogram of the trimodal dataset and the predictive mixture PDF as well as the associated uncertain bounds estimated by the nonparametric Bayesian approach, respectively. For comparison, the results obtained by the parametric Bayesian approach are also provided in Figure 3(a). Noticeable discrepancies are observed between the estimated PDFs of the two approaches, where the nonparametric PDF denoted with a red solid line has higher peaks than the parametric PDF denoted with a grey solid line at around $y = 1$ and $y = 10$. As for cumulative distribution function (CDF), as depicted in Figure 3(b), it is observed that the nonparametric model fits the trimodal dataset better than the parametric model, especially the details at around $y = 1$ and $y = 10$.

To quantitatively compare the efficacy of the nonparametric Bayesian modelling approach and the parametric counterpart, the goodness-of-fit of the estimated PDFs and the computational time required by the two approaches are, respectively, evaluated as shown in Table 1. The goodness-of-fit is measured using two metrics, including the P value of the Kolmogorov–Smirnov test (K-S test) and the log likelihood value, which favor better fitting with a higher value. The results of K-S tests at a significant level of 0.05 fail to reject the null hypotheses for both the nonparametric PDF and the parametric PDF. It should be noted that the P value of the K-S test of the nonparametric PDF is greater than that of the parametric PDF, indicating a higher fitting quality is achieved by the proposed nonparametric Bayesian approach. Similarly, the log likelihood value of the nonparametric PDF is larger than that of the parametric PDF, verifying better goodness-of-fit of the estimated nonparametric model as well. Regarding the computational efficiency, it takes about 4.63 hours to infer the parametric PDF, in which the majority of time is spent on optimal model order selection under multiple candidate models. Since the model order selection is avoided in the process of nonparametric Bayesian inference, the computation time required is 1.66 hours, which is much shorter than that of the parametric counterpart. The computation was performed by the MATLAB platform on a PC with Intel Xeon CPU E5-1620 and 16 GB RAM. From Table 1, it is found that the proposed nonparametric Bayesian modelling approach outperforms the parametric approach in dealing with heterogeneous data in terms of better goodness-of-fit and higher computational efficiency.

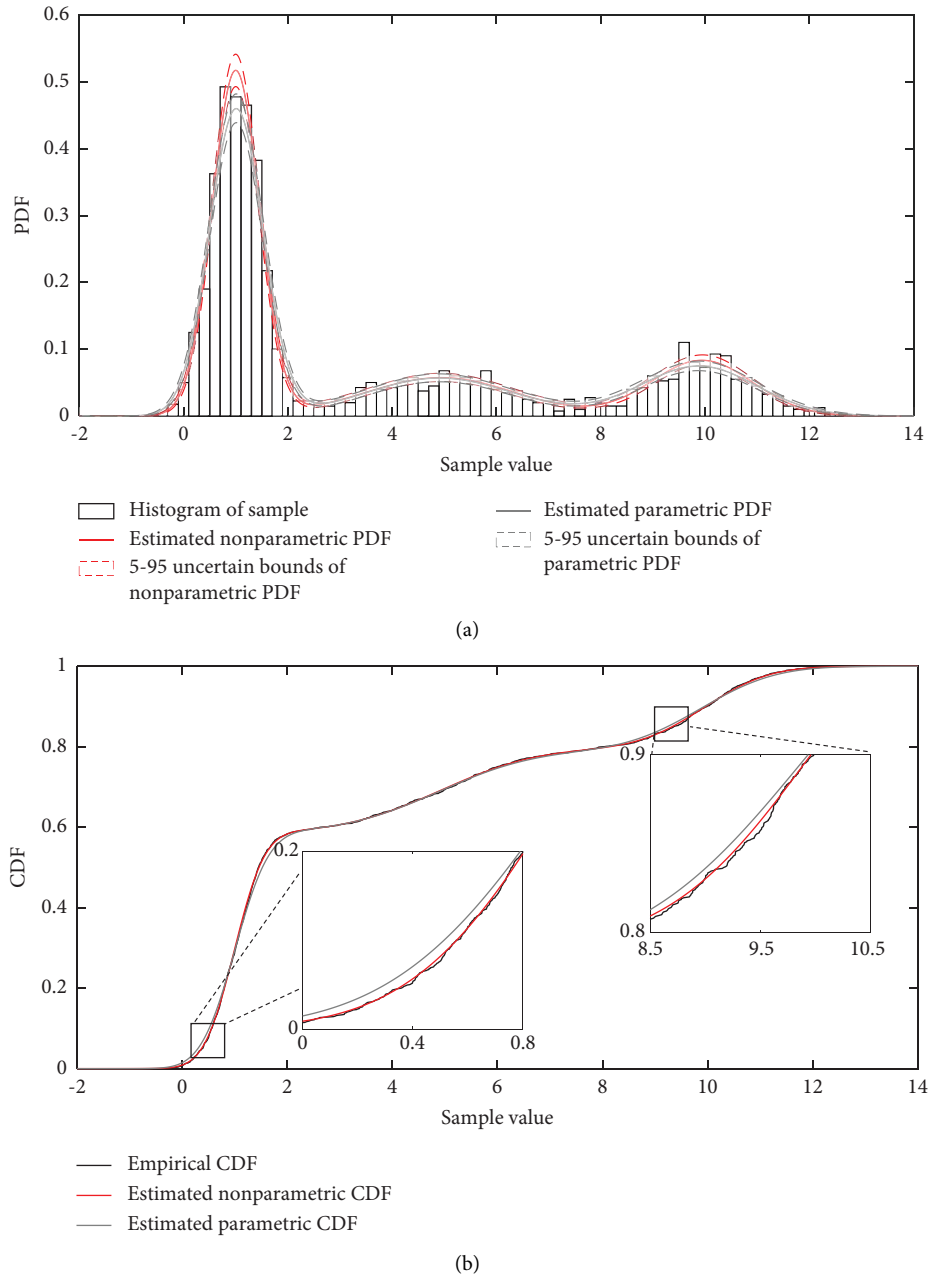

Figure 3: Estimation of the trimodal dataset. (a) PDF. (b) CDF.

Table 1: Comparison of nonparametric and parametric approaches for modelling the trimodal data set.

		Nonparametric approach	Parametric approach
Goodness-of-fit	P value of the K-S test	$9.053e+01$	$2.141e+01$
	Log likelihood value	$-3.867e+03$	$-3.884e+03$
Computation time (hour)		1.66	4.63

5. Application to Tsing Ma Bridge

5.1. Tsing Ma Bridge and Its Strain Monitoring Data. The Tsing Ma Bridge (TMB) as depicted in Figure 4 is a suspension bridge in Hong Kong with a main span of 1377 m and an overall length of 2.16 km, linking the airport and the city center. The bridge has a double-level truss-stiffening box-shape steel deck, where the upper level has a dual three-lane highway and the lower level has two airport railway lines and two emergency lanes, maintaining the diurnal access of the highway and railway vehicles. Being one of the most essential components in the transportation network of

Hong Kong, the TMB was instrumented with a sophisticated long-term SHM system by the Highways Department of the Hong Kong Special Administration Region (SAR) Government since the completion of the bridge construction. Apart from other categories of sensors, a total of 110 strain sensors were deployed at three bridge deck sections, i.e., the middle of the Ma Wan side span, the Ma Wan tower, and the 3/4 of the main span, as highlighted in Figure 4(a). The longitudinal trusses of the bridge deck offer majority of vertical bending stiffness for accommodating the bridge loads; thus, it is a priority to pay attention to the long-term serviceability of the truss elements during routine operation. In a typical monitored cross-section, for example, section CH24662.50, two suites of strain gauges, tagged as SP-TLN-01, SS-TLN-01, SP-TLN-02, SP-TLN-05, and SS-TLN-03 at the north side and tagged as SP-TLS-01, SS-TLS-01, SP-TLS-02, SP-TLS-12, and SS-TLS-09 at the south side were installed on the surfaces of the top chords, diagonal struts, and bottom chords of the longitudinal trusses as illustrated in Figure 5, measuring dynamic strain responses experienced by the bridge. The sampling frequency of the strain data acquisition was set to 51.2 Hz.

One-year monitoring data of strain under routine operation of the TMB are used for this study. Figure 6(a) exemplifies the 12-month raw strain data collected continuously by the sensor SP-TLN-05 deployed at the bottom chord of the north longitudinal truss at section CH24662.50, where the positive value denotes compressive strain and the negative value denotes tension strain. The static strain due to initial dead loads is not measurable since the sensors were installed after the completion of bridge construction. It can be observed from Figure 6(a) that the dynamic strain responses, under the combined action of highway traffic, railway traffic, monsoon, typhoon, and temperature, vary within a range of $-300\ \mu\varepsilon$ to $200\ \mu\varepsilon$ over the year. To investigate the details, a 7-day time history of the strain responses is plotted in Figure 6(b). It is observed that the strain time history exhibits seven cycles notably, each of which represents one-day strain variation as exemplified in Figure 6(c).

The measured strain is relatively small between 2:00 am and 5:00 am as shown in Figure 6(c), since the airport express railway was closed during that period. A low-frequency strain component is observed in the 24-hour raw data, which has been demonstrated to be the effect of daily temperature variation [60]. The thermal strain, although quite large, contributes little to the stress because the majority of it is released by the free movement of bridge deck at the expansion joints. On that account, the thermal strain as absorbed at the expansion joints is excluded from the total strain in subsequent reliability analysis. A wavelet-based multicomponent decomposition procedure [60] is utilized to separate the thermal strain, and the strain response after eliminating the temperature effect for the bottom chord is exemplified in Figure 7.

By multiplying the elastic modulus E of steel, the strain response after eliminating the temperature effect is converted to stress response based on the fact that the bridge is in elastic deformation under routine operation. Figure 8 shows the monitoring-derived stress for the bottom chord under the live loads in a typical 30-minute duration. It is observed that the stress fluctuates rapidly with peaks (negative) that have different amplitudes. The peak values with higher amplitudes are recognized as railway-induced stress response, while the peak values with lower amplitudes are mainly caused by highway traffic. An adaptive peak counting method [61] is then applied to identify the peak stress values from the stress time history to construct the peak stress population in one month as shown in Figure 9(a). It can be seen that the peak stress values are randomly dispersed but mostly clustered to two stress levels. The in-between values among the two stress levels are mainly the effect of normal wind loads. The peak stress values above the higher amplitude level are primarily the results from two scenarios: (i) two trains passing each other in opposite directions on the bridge (approximately two such events occur in one hour) and (ii) strong winds (e.g., typhoons) hitting the bridge in combination with highway/railway traffic. Figure 9(b) shows the histogram of peak stresses in one month, where the stress distribution has notably two peaks, exhibiting a multimodal response feature.

Following the above procedure, the month-by-month peak stress sequences of the top chord, diagonal strut, and bottom chord of the north longitudinal truss at section CH24662.50 are obtained as the live load effects for subsequent reliability assessment.

5.2. Nonparametric Bayesian Estimation of Multimodal Stress. The nonparametric Bayesian modelling approach described in Section 2 is applied to the month-by-month peak stresses to infer their unknown PDFs and to estimate the associated uncertainties. Modelling of stress response of the bottom chord in January is taken as an example to demonstrate the proposed nonparametric Bayesian approach. The collapsed Gibbs sampler is set to run for $T = 10000$ iterations. The mixture PDF samples generated from the collapsed Gibbs sampler in the initial, middle, and final stages are plotted in Figure 10, respectively. It can be seen that, apart from some early draws with flat distributional shapes, the generated mixture PDF samples quickly converge to the target distribution as the iteration continues. To quantitatively examine the convergence of the collapsed Gibbs sampler, the scale reduction factors of the true variance R_T, the within-model variance R_W, and the between-model variance R_B are computed along with the iterations. Figure 11 shows that all the scale reduction factors quickly approach one, certifying the convergence of the collapsed Gibbs sampler performed. The convergence statistics are listed in Table 2, where the scale reduction factor of the true variance R_T needs more iterations than the other two factors to decline to one. Based on the convergence statistics, the burn-in period for the Gibbs iterations is determined as $B = 5000$, and the remaining $G = T - B = 5000$ samples from the Gibbs iterations are regarded as posterior mixture PDF samples, which are then used to construct the PDF of the peak stresses.

The model order of the DPGMM is a random variable such that it keeps varying along with the iterations of the collapsed Gibbs sampler. Figure 12 shows the variation of

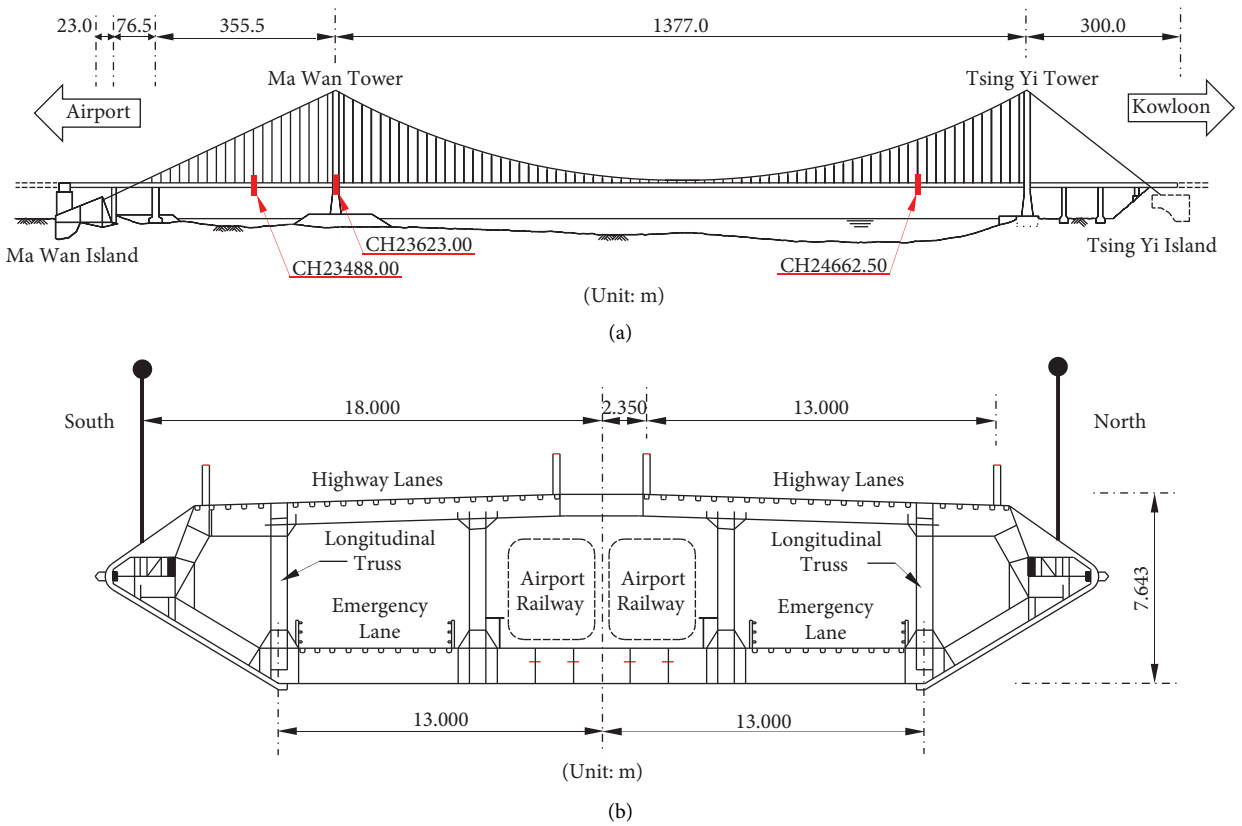

Figure 4: Layout of TMB and strain monitoring sections. (a) Deck sections instrumented with strain sensors. (b) Deck cross-section.

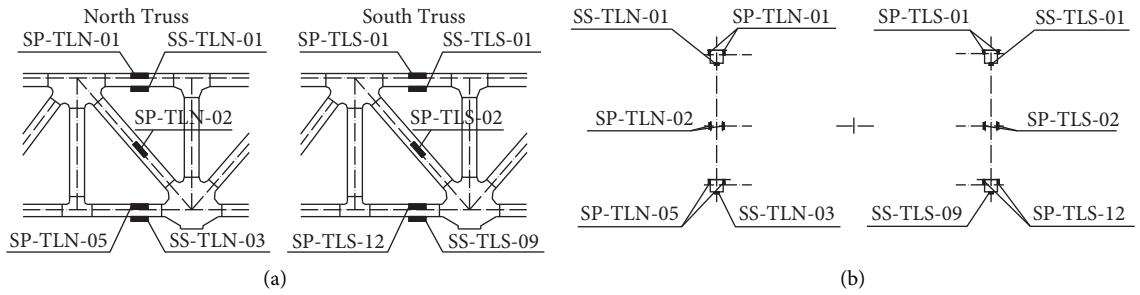

Figure 5: Deployment of strain sensors on longitudinal trusses. (a) Elevation view. (b) Cross-sectional view.

model order K of the generated mixture PDF samples through the entire Gibbs run and the distribution of K after burn-in period for modelling the peak stresses at the bottom chord in January. It can be seen that the values of the model order are relatively small in the early stage, thus producing flat distribution samples as indicated in Figure 10(a). It then becomes larger and reaches to stationarity after the burn-in period. The most frequently occurring model order for the bottom chord is $K = 9$ as observed from the histogram in Figure 12. As can be seen from Figures 10 and 12, after the burn-in period, the posterior mixture PDF samples with higher model order can better depict the target distribution of peak stresses.

After obtaining the posterior mixture PDF samples, the predictive mixture PDF and the associated uncertain bounds can be evaluated by using equations (19) and (20), respectively. Figure 13 plots the estimated predictive mixture PDFs and their associated 5–95 uncertain bounds of the multimodal stress responses for the top chord, diagonal strut, and bottom chord in January, respectively. Results obtained by the parametric approach are also provided in Figure 13 for comparison. It is observed that the estimated nonparametric PDFs represented by red solid lines fit the stress histograms better than the parametric PDFs denoted by grey solid lines for all the three truss members. It is worth mentioning that the nonparametric approach performs better in the tail part modelling of stress distributions, which has a marked influence on the evaluation of failure probability. Table 3 compares the model orders used in and the goodness-of-fit of the two approaches. It is found that the nonparametric approach tends to adopt more components in mixture modelling for the three truss members. The

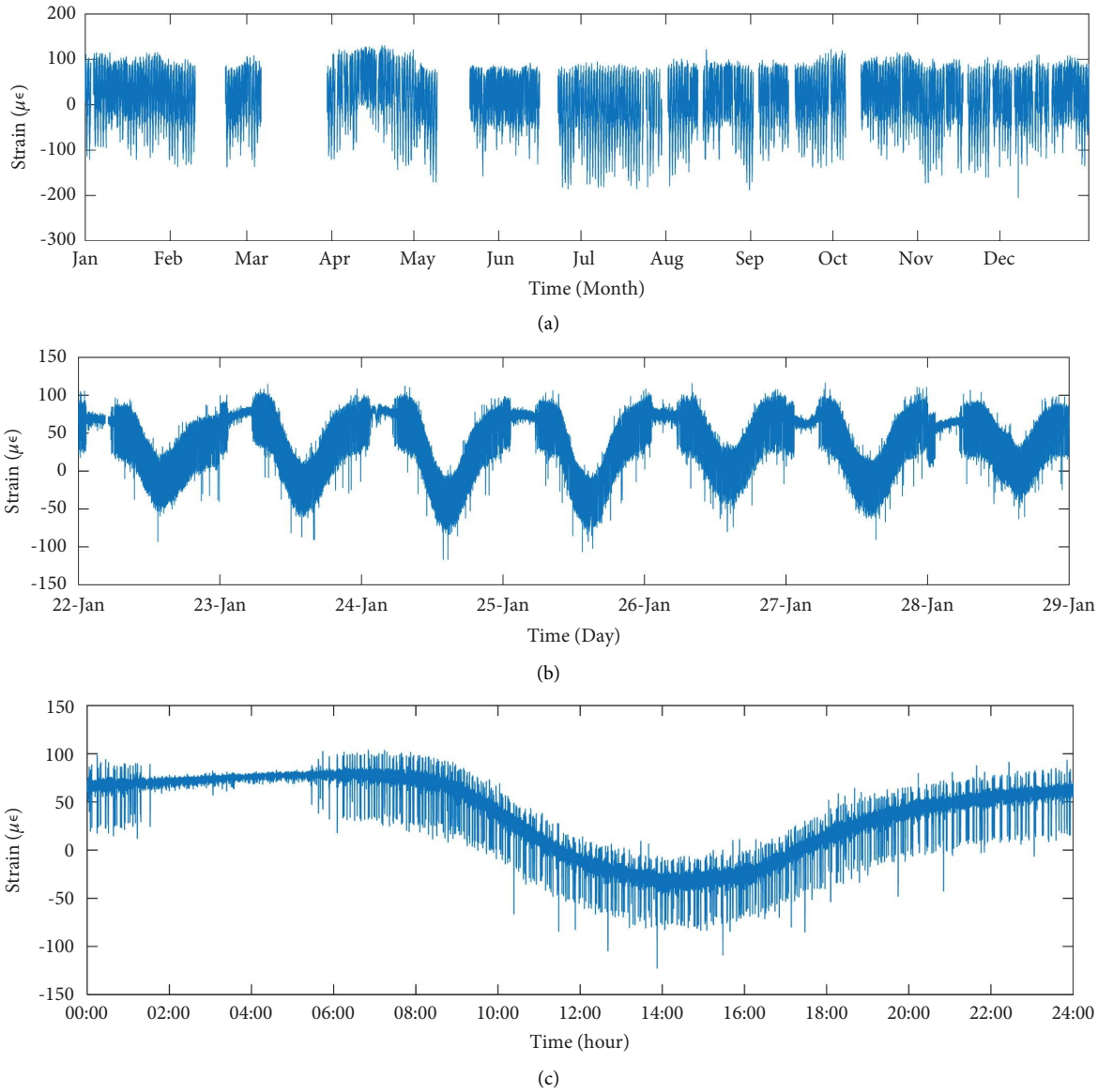

Figure 6: Raw strain data measured at bottom chord of north longitudinal truss. (a) Annual strain. (b) Weekly strain. (c) Daily strain.

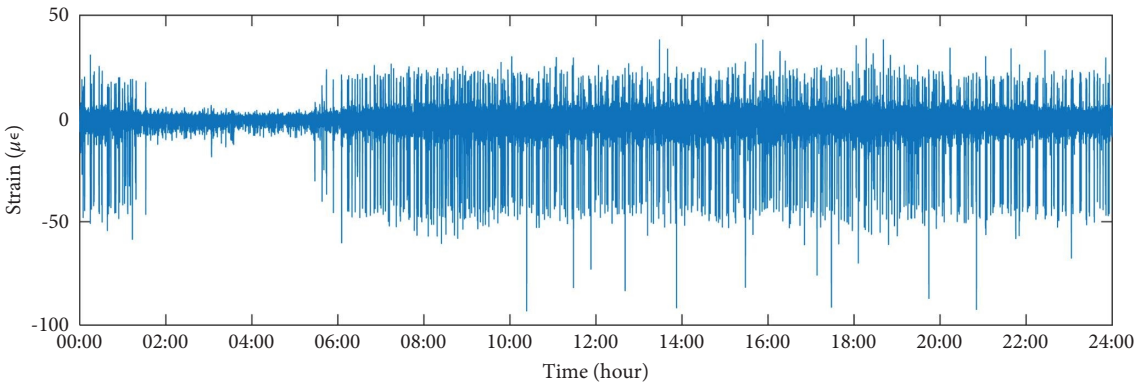

Figure 7: Strain after eliminating temperature-induced effect.

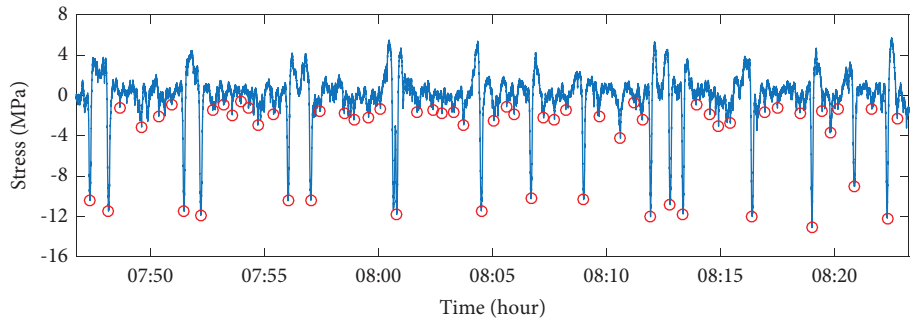

FIGURE 8: Stress response and identified peak stresses in 30 minutes.

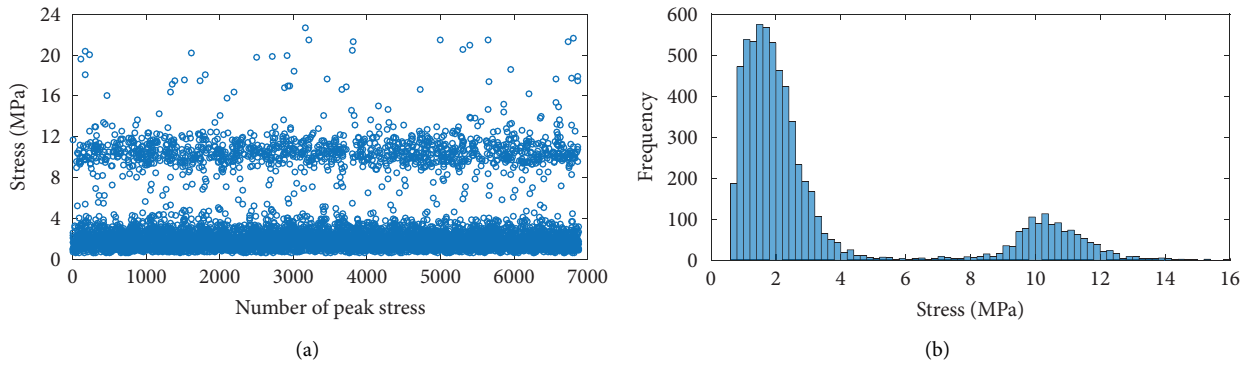

FIGURE 9: Extracted peak stresses in one-month duration. (a) Peak stress sequence. (b) Histogram of peak stresses.

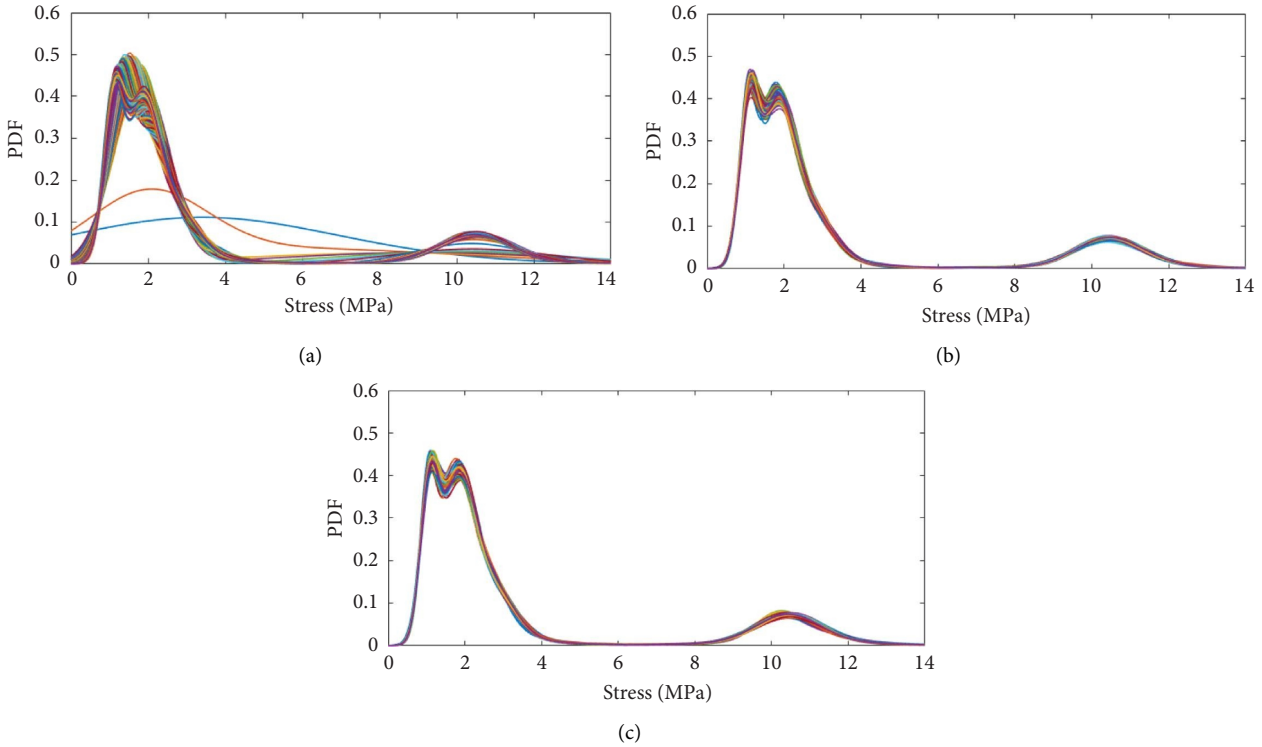

FIGURE 10: Posterior mixture PDF samples generated from Gibbs iterations. (a) Initial stage ($t = 1:1000$). (b) Middle stage ($t = 5001:6000$). (c) Final stage ($t = 9001:10000$).

goodness-of-fit is evaluated with the P value of the K-S test and the log likelihood value, respectively. Both the P value and the log likelihood value of the nonparametric models are noticeably higher than those of the parametric models, verifying that a better fitting quality is achieved by the proposed approach. In Figure 13, the 5–95 uncertain bounds depicted by red dotted lines unveil the variability in PDF estimation due to the model order and parameter uncertainties as considered in the nonparametric approach.

5.3. Evolutionary Reliability Assessment under Modelling Uncertainties. As stipulated in the design documents of the TMB, the maximum allowable stress of the truss members under live loads in serviceability limit state is 60 MPa [62]. The coefficient of variation for the designed maximum allowable stress is taken as 0.075 in this study [4, 63]. Consequently, the mean value and the standard deviation of the structural resistance R are determined as $\mu_R = 60$ MPa and $\sigma_R = 4.5$ MPa for assessment, respectively. It should be noted that if durability-relevant sensors are deployed on the bridge of concern, the probability model for structural resistance can be formulated with the nonparametric Bayesian approach from the monitoring data accordingly.

With the nonparametric estimation of the monitored live load effect (peak stress), the samples of the conditional reliability index can be obtained by using equation (28). Then, the sample mean and the sample standard deviation (SD) can be evaluated by using equations (29) and (30), respectively. Table 4 lists the mean values and the SDs of reliability estimates for the top chord, diagonal strut, and bottom chord in January using the estimated nonparametric mixture models as shown in Figure 13. It can be seen that the diagonal strut owns the highest reliability index (mean = 11.079 and SD = 0.270), the top chord comes to the second (mean = 9.954 and SD = 0.236), and the bottom chord has the lowest reliability index (mean = 8.621, SD = 0.304), which are consistent with the observed stress level experienced by each truss member as shown in Figure 13. The reliability estimates obtained by the parametric approach are also provided in Table 4 for comparison. The mean values of reliability indices for the top and bottom chords from the nonparametric approach are higher than those obtained by the parametric counterpart, while as for the diagonal strut, the result is opposite. Notice that the variabilities (in terms of SDs) of reliability indices estimated by the nonparametric approach are larger than those of the parametric counterpart for all truss members. This is attributed to the fact that both the parameter uncertainty and the model order uncertainty of the mixture model have been taken into account in the nonparametric approach.

In fact, the extent of variability in the reliability estimate induced by modelling uncertainties is in close relation to the size of the monitoring dataset used. It is assumed that the sampling frequency of strain sensors is adjustable, and peak stress datasets with different sample sizes are acquired in the same month. Figure 14 gives the relationships between the sample size of peak stresses and the estimated conditional reliability index for top chord using the nonparametric and parametric approaches, respectively. It can be observed that, the larger the sample size of peak stresses, the narrower the uncertainty of reliability estimates under both approaches. As shown in Figure 14(b), when the sample size of peak stresses is smaller than 3000, the reliability estimate obtained from the parametric approach fluctuates with large uncertain bounds. It indicates that if monitoring data are insufficient, misleading assessment result can be delivered. The nonparametric approach, as shown in Figure 14(a), outperforms the parametric counterpart in estimating the reliability index under the situation of insufficient peak stress samples. It is attributed to the fact that the nonparametric Bayesian mixture model without model order constraint avoids biased fitting when there is lack of monitoring data. From the bridge owner's point of view, if the estimated uncertainty of reliability is too large for decision-making, proper actions should be taken to collect additional information (e.g., increasing the sampling frequency) to assist the bridge assessment. However, a compromise should be made between the acceptability of uncertainty level for assessment and the cost to collect additional data.

With successively collected monitoring data, the reliability estimate is routinely updated by using the Bayesian updating formulas (31) and (32). Figure 15 illustrates the updating of reliability estimates from January to February for the top chord, diagonal strut, and bottom chord based on the nonparametric approach. Taking the reliability updating of the top chord in Figure 15(a) as an example, the blue solid line is the reliability assessment result in January with the mean and the SD same as those given in Table 4. As monitoring data in February accumulate, the samples of the conditional reliability index in February are first obtained by using equation (28) with the elicited distribution denoted by the grey dotted line. The predictive reliability index in February is then evaluated by updating the distribution of the conditional reliability index in February (serving as likelihood) with the preceding reliability distribution in January (serving as prior), and the resulting distribution is depicted by the red solid line. It can be seen from Figure 15 that the updated reliability estimates fall in between the newly obtained conditional reliability indices and the preceding reliability estimates for the top chord, diagonal strut, and bottom chord. Following the same procedure, since one-year monitoring data are available in this case study, the reliability estimates are updated month-by-month as shown in Figure 16, with the use of nonparametric Bayesian mixture models constructed with the use of monthly monitoring data. The predictive reliability indices in December denoted by the red solid line incorporate historical reliability indices from January to November denoted by grey solid lines, which can be viewed as the one-year reliability assessment results of the truss members.

Based on the month-by-month updating results, the one-year evolution of the predictive reliability indices and the associated uncertain bounds for the top chord, diagonal strut, and bottom chord is shown in Figure 17. It is observed that the means and SDs of the predictive reliability indices under routine operation of the bridge attain almost to stationarity after updating with the monitoring data

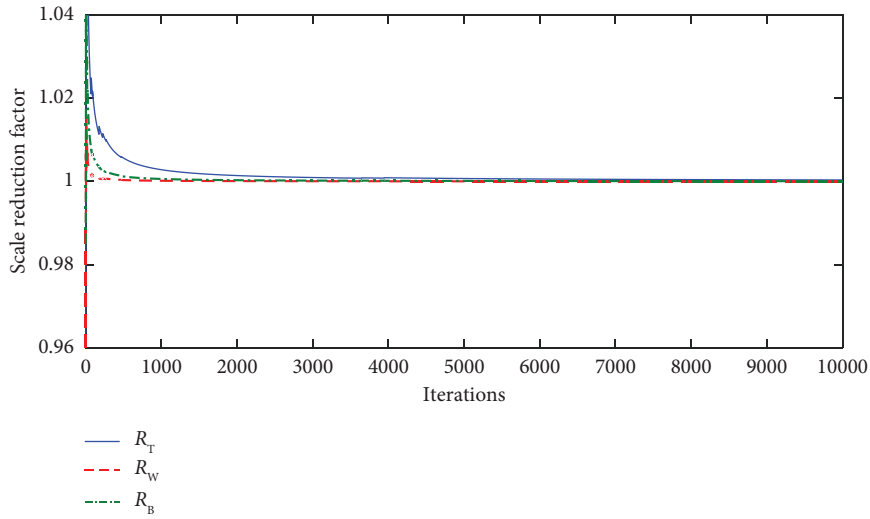

Figure 11: Convergence monitoring of the collapsed Gibbs sampler.

Table 2: Convergence statistics of the collapsed Gibbs sampler.

R_T	R_W	R_B
Gibbs iterations needed to reach convergence $\lvert R-1\rvert < 10^{-3}$		
2819	148	595

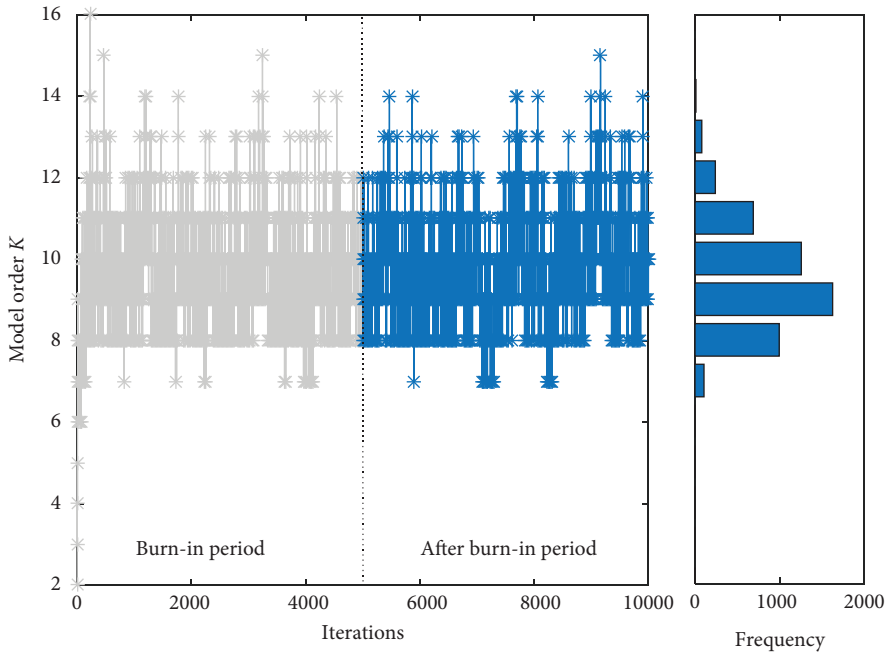

Figure 12: Variation of model order through Gibbs iterations.

acquired in July. Before that, the predictive reliability indices obtained in March are notably different from those in other months with deviated means and enlarged SDs. The reason is the insufficient SHM data collected in March because the data acquisition system was malfunctioning for days in that month [64]. This finding verifies again that the sample size of monitoring data has considerable effect on the estimated reliability index. As evidenced by Figure 17, although the short-term assessment result may be affected by adverse factors such as lack of monitoring data, the sample size-induced deviation of the reliability estimate can be gradually diminished with the successively acquired data by using the Bayesian updating procedure.

After being stationary of the predictive reliability indices, the SDs for the truss members are almost identical, ranging from 0.3 to 0.5. The means for them are different, among

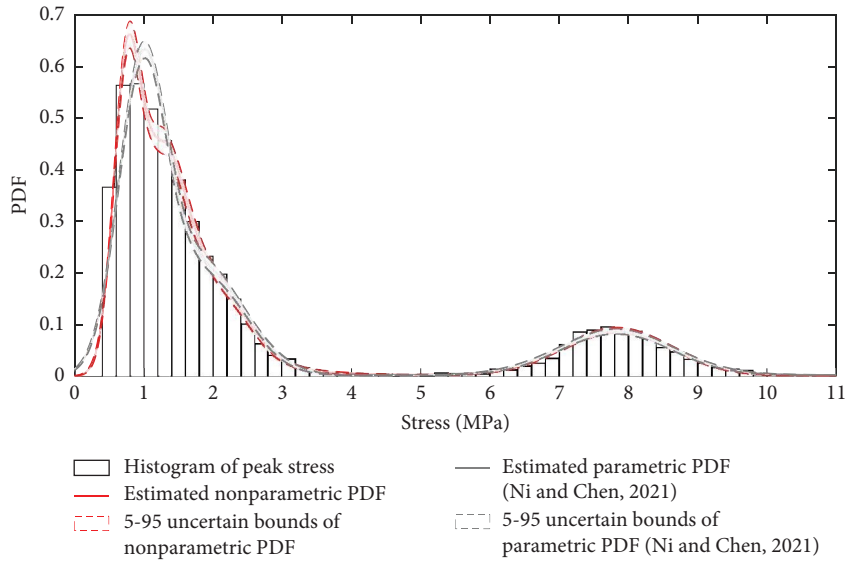

(a)

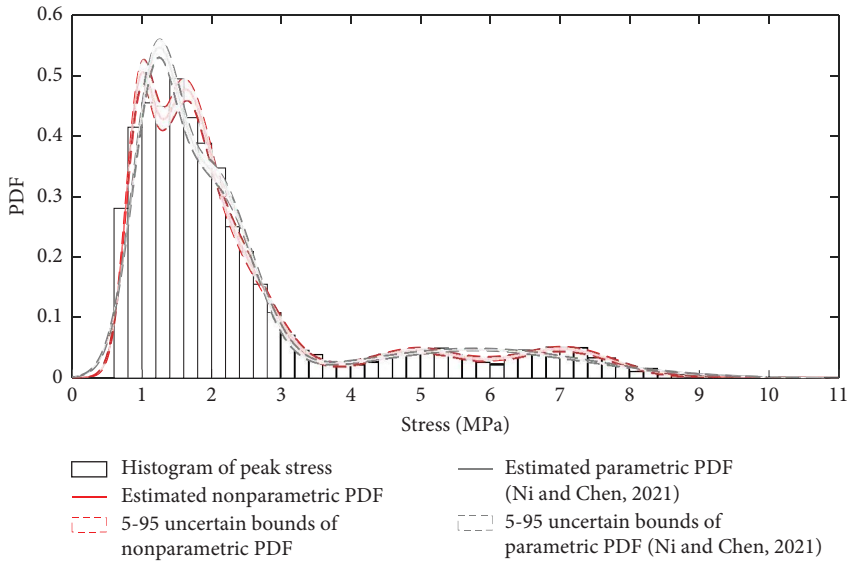

(b)

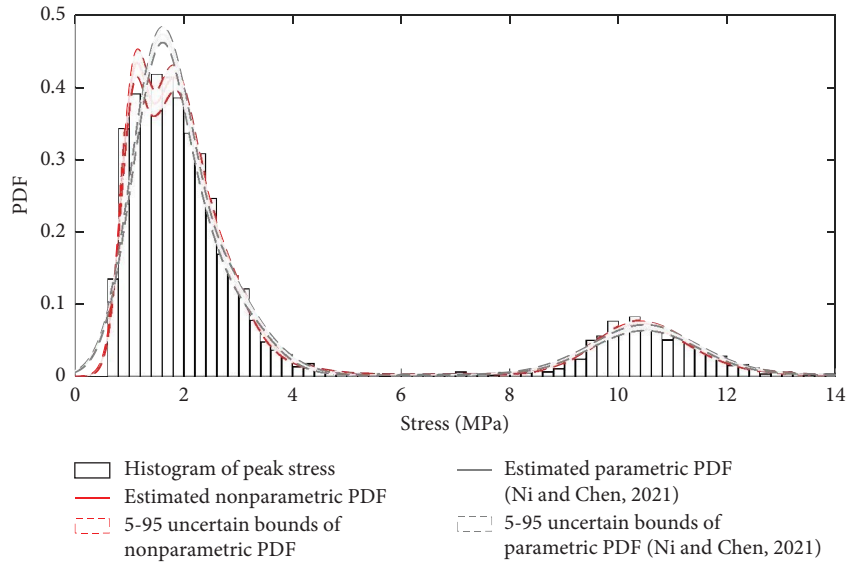

(c)

Figure 13: Estimated mixture PDFs with uncertain bounds of stress responses. (a) Top chord. (b) Diagonal strut. (c) Bottom chord.

Table 3: Comparison of nonparametric and parametric approaches for modelling of multimodal stress responses.

Truss member	Nonparametric approach	Parametric approach
	Model order	
Top chord	8	4
Diagonal strut	8	3
Bottom chord	9	4
	P value of the K-S test	
Top chord	$7.730e-02$	$1.050e-06$
Diagonal strut	$1.488e-01$	$1.500e-03$
Bottom chord	$6.933e-01$	$5.974e-04$
	Log likelihood value	
Top chord	$-9.777e+03$	$-9.963e+03$
Diagonal strut	$-1.135e+04$	$-1.152e+04$
Bottom chord	$-1.176e+04$	$-1.195e+04$

Note. The most frequently occurring model orders are listed in the nonparametric approach, while the Bayes factor-based optimal model orders are listed in the parametric approach.

Table 4: Comparison of nonparametric and parametric approaches on the conditional reliability index.

Truss member	Conditional reliability index			
	Nonparametric approach		Parametric approach	
	Mean	SD	Mean	SD
Top chord	9.954	0.236	9.089	0.218
Diagonal strut	11.079	0.270	11.482	0.032
Bottom chord	8.621	0.304	7.882	0.207

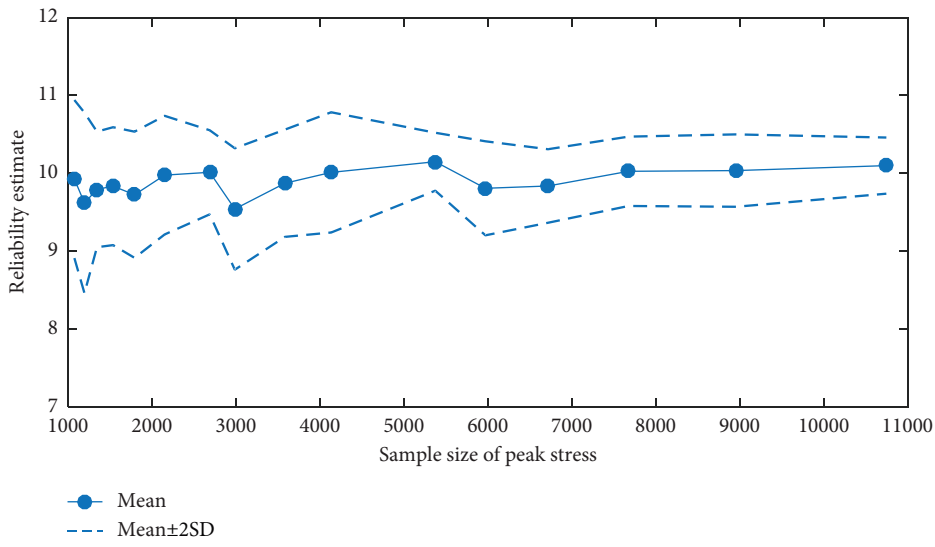

(a)

Figure 14: Continued.

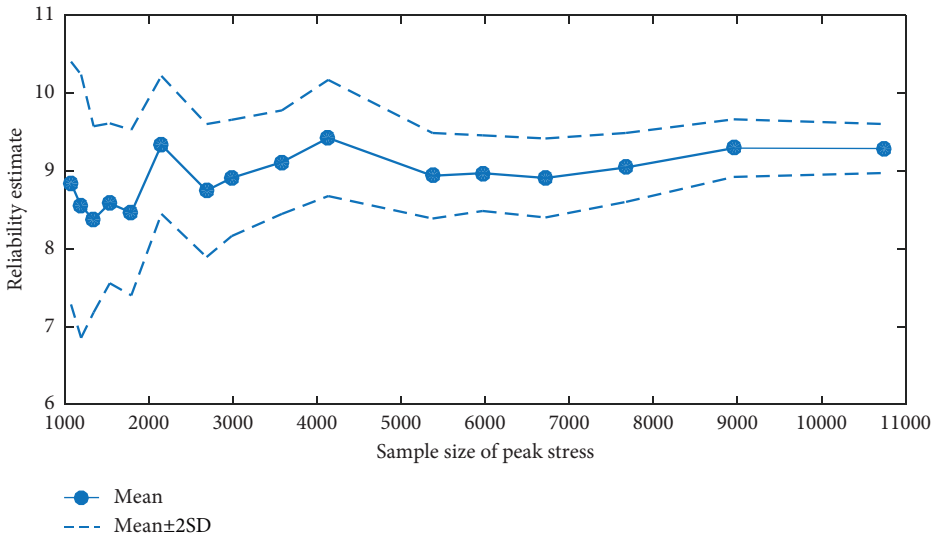

(b)

FIGURE 14: The relationship between the sample size of peak stresses and the conditional reliability index. (a) Nonparametric approach. (b) Parametric approach.

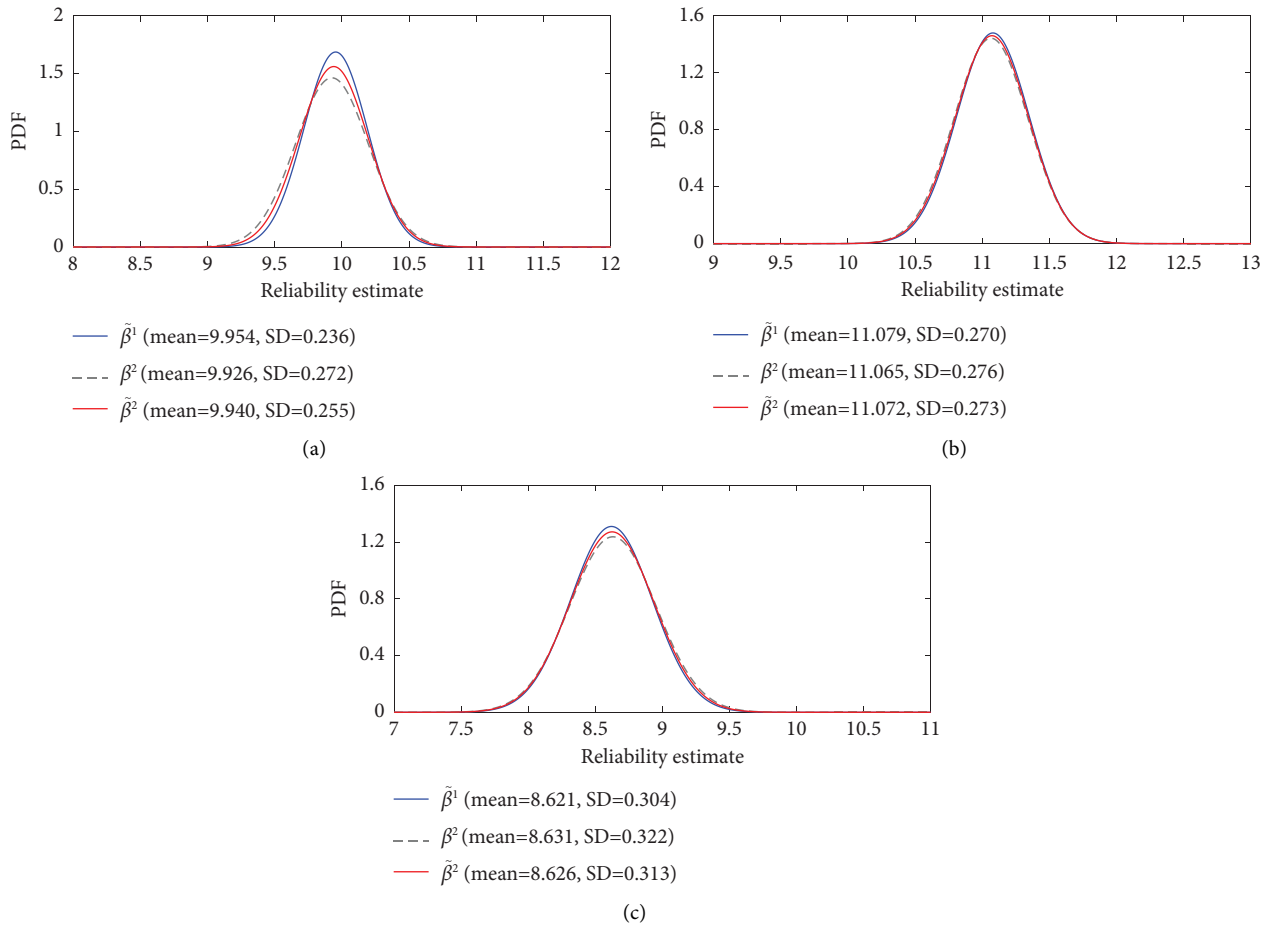

FIGURE 15: One-month reliability updating. (a) Top chord. (b) Diagonal strut. (c) Bottom chord.

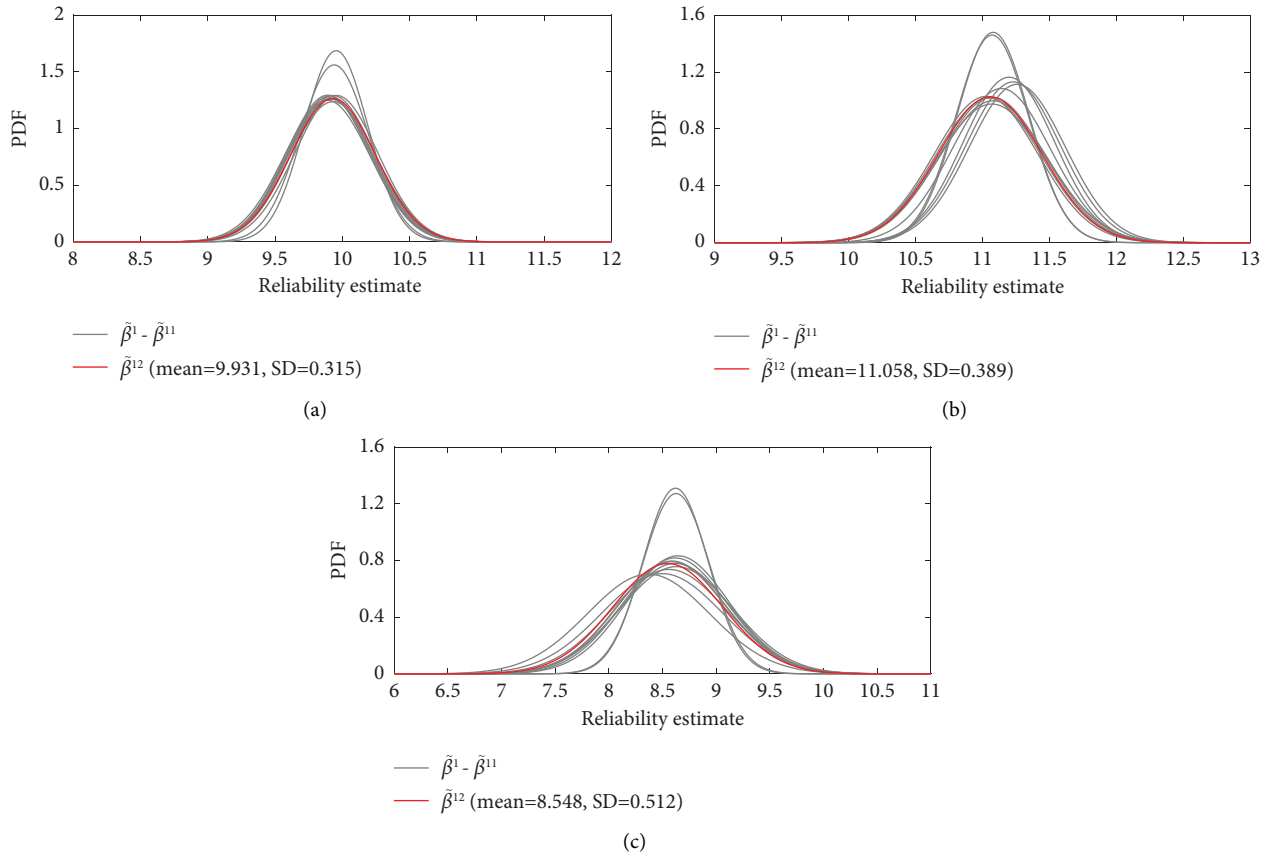

Figure 16: One-year reliability updating. (a) Top chord. (b) Diagonal strut. (c) Bottom chord.

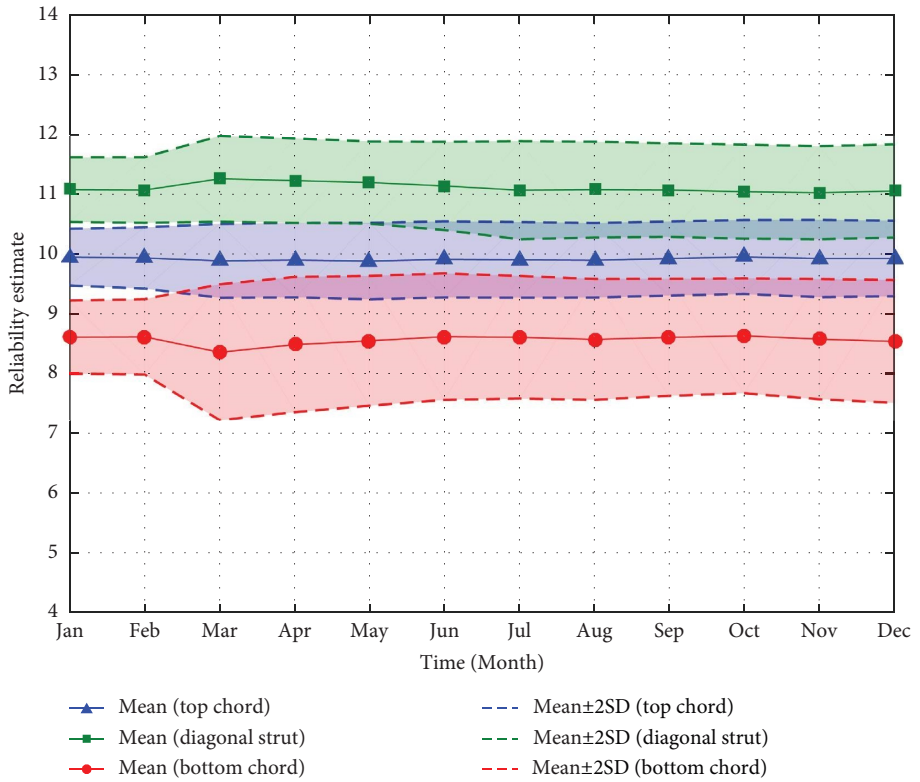

Figure 17: Evolution of predictive reliability indices in one year.

Table 5: Relationship between the reliability index and maintenance action [65].

Safety state	5	4	3	2	1
Reliability index	$\beta \geq 9.0$	$9.0 > \beta \geq 8.0$	$8.0 > \beta \geq 6.0$	$6.0 > \beta \geq 4.6$	$4.6 > \beta$
Attribute for safety	Excellent	Very good	Good	Fair	Unacceptable
Maintenance action	No action	Preventive inspection	Detailed inspection	Possible strengthening	Rehabilitation

which the diagonal strut has the highest mean, the top chord comes to the second, and the bottom chord owns the lowest mean. Table 5 gives the relationship between the reliability index and the maintenance action [65]. By judging on the mean curves of predictive reliability indices shown in Figure 17, it is recognized that the diagonal strut (mean > 11) and the top chord (mean > 9.5) are in excellent condition with no need of inspection; the bottom chord (mean > 8) is in very good condition that only the preventive inspection is needed. The upper and lower uncertain bounds of the predictive reliability indices provide additional valuable information on the safety assessment, helping bridge owners to schedule and prioritize inspection and maintenance actions in consideration of various uncertainties and potential risks.

6. Conclusions

This study presented a nonparametric Bayesian mixture model-based approach for reliability assessment of in-service bridges using long-term monitoring data. The advantage brought by the nonparametric Bayesian inference is that the model complexity can freely adapt to the size of observed data so that there is no need to make assumption of the model order in advance of inference, thereby avoiding tedious model selection. Statistical modelling using the nonparametric Bayesian mixture model for multimodal stress responses retrieves concurrently the most plausible model order and the most plausible PDF, as well as their associated uncertainties. The conditional reliability index elicited with the nonparametric Bayesian model enables both the aleatory and epistemic uncertainties arising from resistance and load effect characterization to be accounted for, whilst it can be successively updated with accumulated monitoring data to realize an evolutionary reliability assessment.

After verifying the effectiveness of the nonparametric Bayesian approach in modelling heterogeneous data with a numerical example, a case study using one-year strain monitoring data collected from the instrumented Tsing Ma Bridge was demonstrated to examine the feasibility of the proposed reliability assessment procedure. The results come to the following conclusions/observations: (i) the nonparametric Bayesian mixture model without model order constraint outperforms the parametric counterpart in characterization of heterogeneous monitoring data, and the reliability estimate by the nonparametric Bayesian model is more robust in the situation of insufficient data; (ii) the uncertainty in reliability estimate is in close relation with the volume of monitoring data, i.e., increasing the sample size helps to mitigate the uncertainty of the reliability estimate, and a compromise should be made by the authority between the acceptability of uncertainty level for assessment and the cost of collecting additional monitoring data; (iii) the short-term lack of monitoring data due to system malfunction may induce bias in the reliability estimate as well as high uncertainty, but the adverse effects can be trimmed down by subsequently collected data with execution of the Bayesian updating strategy; (iv) in compliance with an accepted risk criterion, the estimated reliability indices (including the means and SDs) for various structural components offer an effective instruction for scheduling and prioritizing bridge inspection and maintenance activities.

Appendix

A. Formulation of Variances for Quantitative Convergence Diagnosis of the Collapsed Gibbs Sampler

In this appendix, five types of variances of ϕ are derived for use in quantitative convergence diagnosis of the collapsed Gibbs sampler [59]. Suppose a total of L chains of ϕ are produced and let $\phi_l^{(t)}$ denote the value in the lth chain at the tth iteration. The total variance of ϕ can be estimated as follows:

$$V = \frac{1}{LT-1} \sum_{l=1}^{L} \sum_{t=1}^{T} \left(\phi_l^{(t)} - \overline{\phi}\right)^2, \tag{A1}$$

where

$$\overline{\phi} = \frac{1}{LT} \sum_{l=1}^{L} \sum_{t=1}^{T} \phi_l^{(t)}. \tag{A2}$$

Suppose a total of M models are visited across the chains during the iterations and let T_{lm} denote the number of times that the mth model is visited in the l th chain. Accordingly, let $\phi_{lm}^{(t)}$ denote the t th value of the m th model in the l th chain, and $t = 1, \cdots, T_{lm}$. Then, the within-chain variance W_c, the within-model variance W_m, the variance within both chains and models $W_m W_c$, the between-model variance B_m, and the within-chain variance split between and averaged over models $B_m W_c$ of ϕ can be, respectively, constructed as follows:

$$W_c = \frac{1}{L}\sum_{l=1}^{L}\sum_{m=1}^{M}\sum_{t=1}^{T_{lm}}\frac{\left(\phi_{lm}^{(t)}-\overline{\phi}_l\right)^2}{MT_l-1},$$

$$W_m = \frac{1}{M}\sum_{l=1}^{L}\sum_{m=1}^{M}\sum_{t=1}^{T_{lm}}\frac{\left(\phi_{lm}^{(t)}-\overline{\phi}_m\right)^2}{LT_m-1},$$

$$W_mW_c = \frac{1}{LM}\sum_{l=1}^{L}\sum_{m=1}^{M}\sum_{t=1}^{T_{lm}}\frac{\left(\phi_{lm}^{(t)}-\overline{\phi}_{lm}\right)^2}{T_{lm}-1}, \tag{A3}$$

$$B_m = \sum_{m=1}^{M}\frac{\left(\overline{\phi}_m-\overline{\phi}\right)^2}{M-1},$$

$$B_mW_c = \sum_{l=1}^{L}\sum_{m=1}^{M}\frac{\left(\overline{\phi}_{lm}-\overline{\phi}_l\right)^2}{L(M-1)},$$

where

$$T_l = \sum_{m=1}^{M}T_{lm},$$

$$T_m = \sum_{l=1}^{L}T_{lm},$$

$$\overline{\phi}_l = \frac{1}{T_l}\sum_{m=1}^{M}\sum_{t=1}^{T_{lm}}\phi_{lm}^{(t)}, \tag{A4}$$

$$\overline{\phi}_m = \frac{1}{T_m}\sum_{l=1}^{L}\sum_{t=1}^{T_{lm}}\phi_{lm}^{(t)},$$

$$\overline{\phi}_{lm} = \frac{1}{T_{lm}}\sum_{t=1}^{T_{lm}}\phi_{lm}^{(t)}.$$

Data Availability

The data used to support the findings of this study are available from the corresponding author upon request.

Conflicts of Interest

The authors declare that they have no conflicts of interest.

Acknowledgments

This work was supported by the Research Grants Council of the Hong Kong Special Administrative Region, China, grant no. PolyU 152241/15E; the Innovation and Technology Commission of the Hong Kong Special Administrative Region Government, grant no. K-BBY1; and the National Natural Science Foundation of China, grant no. U1934209.

References

[1] Y. Mori and B. R. Ellingwood, "Reliability-based service-life assessment of aging concrete structures," *Journal of Structural Engineering*, vol. 119, no. 5, pp. 1600–1621, 1993.

[2] A. E. Aktan, D. N. Farhey, D. L. Brown et al., "Condition assessment for bridge management," *Journal of Infrastructure Systems*, vol. 2, no. 3, pp. 108–117, 1996.

[3] F. N. Catbas, M. Susoy, and D. M. Frangopol, "Structural health monitoring and reliability estimation: long span truss bridge application with environmental monitoring data," *Engineering Structures*, vol. 30, no. 9, pp. 2347–2359, 2008.

[4] D. M. Frangopol, A. Strauss, and S. Kim, "Bridge reliability assessment based on monitoring," *Journal of Bridge Engineering*, vol. 13, no. 3, pp. 258–270, 2008.

[5] Y. Q. Ni, X. W. Ye, and J. M. Ko, "Monitoring-based fatigue reliability assessment of steel bridges: analytical model and application," *Journal of Structural Engineering*, vol. 136, no. 12, pp. 1563–1573, 2010.

[6] S. L. Li, S. Y. Zhu, Y. L. Xu, Z. W. Chen, and H. Li, "Long-term condition assessment of suspenders under traffic loads based on structural monitoring system: application to the Tsing Ma Bridge," *Structural Control and Health Monitoring*, vol. 19, no. 1, pp. 82–101, 2012b.

[7] L. Sun, Z. Shang, Y. Xia, S. Bhowmick, and S. Nagarajaiah, "Review of bridge structural health monitoring aided by big data and artificial intelligence: from condition assessment to damage detection," *Journal of Structural Engineering*, vol. 146, no. 5, Article ID 04020073, 2020.

[8] F. N. Catbas and A. E. Aktan, "Condition and damage assessment: issues and some promising indices," *Journal of Structural Engineering*, vol. 128, no. 8, pp. 1026–1036, 2002.

[9] A. A. Mufti, "Structural health monitoring of innovative canadian civil engineering structures," *Structural Health Monitoring*, vol. 1, no. 1, pp. 89–103, 2002.

[10] J. M. Ko and Y. Q. Ni, "Technology developments in structural health monitoring of large-scale bridges," *Engineering Structures*, vol. 27, no. 12, pp. 1715–1725, 2005.

[11] J. M. W. Brownjohn, "Structural health monitoring of civil infrastructure," *Philosophical Transactions of the Royal Society A: Mathematical, Physical & Engineering Sciences*, vol. 365, no. 1851, pp. 589–622, 2007.

[12] J. P. Ou and H. Li, "Structural health monitoring in mainland China: review and future trends," *Structural Health Monitoring*, vol. 9, no. 3, pp. 219–231, 2010.

[13] Y. Fujino and D. M. Siringoringo, "Bridge monitoring in Japan: the needs and strategies," *Structure and Infrastructure Engineering*, vol. 7, no. 7-8, pp. 597–611, 2011.

[14] D. V. Val, M. G. Stewart, and R. E. Melchers, "Life-cycle performance of RC bridges: probabilistic approach," *Computer-Aided Civil and Infrastructure Engineering*, vol. 15, no. 1, pp. 14–25, 2000.

[15] Y. Q. Ni, X. G. Hua, and J. M. Ko, "Reliability-based assessment of bridges using long-term monitoring data," *Key Engineering Materials*, vol. 321–323, pp. 217–222, 2006.

[16] M. Liu, D. M. Frangopol, and S. Kim, "Bridge safety evaluation based on monitored live load effects," *Journal of Bridge Engineering*, vol. 14, no. 4, pp. 257–269, 2009.

[17] H. Li, S. L. Li, J. P. Ou, and H. W. Li, "Reliability assessment of cable-stayed bridges based on structural health monitoring

techniques," *Structure and Infrastructure Engineering*, vol. 8, no. 9, pp. 829–845, 2012a.

[18] H. W. Xia, Y. Q. Ni, K. Y. Wong, and J. M. Ko, "Reliability-based condition assessment of in-service bridges using mixture distribution models," *Computers & Structures*, vol. 106-107, pp. 204–213, 2012.

[19] E. J. Obrien, F. Schmidt, D. Hajializadeh et al., "A review of probabilistic methods of assessment of load effects in bridges," *Structural Safety*, vol. 53, pp. 44–56, 2015.

[20] G. McLachlan and D. Peel, *Finite Mixture Models*, John Wiley & Sons, New York, NY, USA, 2000.

[21] S. Frühwirth-Schnatter, *Finite Mixture and Markov Switching Models*, Springer Science & Business Media, Berlin, Germany, 2006.

[22] Y. Q. Ni, X. W. Ye, and J. M. Ko, "Modeling of stress spectrum using long-term monitoring data and finite mixture distributions," *Journal of Engineering Mechanics*, vol. 138, no. 2, pp. 175–183, 2012b.

[23] E. J. Obrien, A. Bordallo-Ruiz, and B. Enright, "Lifetime maximum load effects on short-span bridges subject to growing traffic volumes," *Structural Safety*, vol. 50, pp. 113–122, 2014.

[24] S. L. Li, S. Y. Wei, Y. Q. Bao, and H. Li, "Condition assessment of cables by pattern recognition of vehicle-induced cable tension ratio," *Engineering Structures*, vol. 155, pp. 1–15, 2018.

[25] X. W. Ye, P. S. Xi, Y. H. Su, B. Chen, and J. P. Han, "Stochastic characterization of wind field characteristics of an arch bridge instrumented with structural health monitoring system," *Structural Safety*, vol. 71, pp. 47–56, 2018.

[26] A. Gelman, J. B. Carlin, H. S. Stern, D. B. Dunson, A. Vehtari, and D. B. Rubin, *Bayesian Data Analysis*, CRC Press, New York, NY, USA, 2014.

[27] J. L. Beck and L. S. Katafygiotis, "Updating models and their uncertainties. I: Bayesian statistical framework," *Journal of Engineering Mechanics*, vol. 124, no. 4, pp. 455–461, 1998.

[28] L. S. Katafygiotis, C. Papadimitriou, and H. F. Lam, "A probabilistic approach to structural model updating," *Soil Dynamics and Earthquake Engineering*, vol. 17, no. 7-8, pp. 495–507, 1998.

[29] B. Goller and G. I. Schueller, "Investigation of model uncertainties in Bayesian structural model updating," *Journal of Sound and Vibration*, vol. 330, no. 25, pp. 6122–6136, 2011.

[30] X. Jiang, S. Mahadevan, and H. Adeli, "Bayesian wavelet packet denoising for structural system identification," *Structural Control and Health Monitoring*, vol. 14, no. 2, pp. 333–356, 2007.

[31] S. K. Au, "Fast Bayesian FFT method for ambient modal identification with separated modes," *Journal of Engineering Mechanics*, vol. 137, no. 3, pp. 214–226, 2011.

[32] S. K. Au, F. L. Zhang, and Y. C. Ni, "Bayesian operational modal analysis: theory, computation, practice," *Computers & Structures*, vol. 126, pp. 3–14, 2013.

[33] K. V. Yuen and H. Q. Mu, "Real-time system identification: an algorithm for simultaneous model class selection and parametric identification," *Computer-Aided Civil and Infrastructure Engineering*, vol. 30, no. 10, pp. 785–801, 2015.

[34] H. P. Wan and Y. Q. Ni, "Bayesian modeling approach for forecast of structural stress response using structural health monitoring data," *Journal of Structural Engineering*, vol. 144, no. 9, Article ID 04018130, 2018.

[35] H. Sohn and K. H. Law, "A Bayesian probabilistic approach for structure damage detection," *Earthquake Engineering & Structural Dynamics*, vol. 26, no. 12, pp. 1259–1281, 1997.

[36] J. L. Beck, S. K. Au, and M. W. Vanik, "Monitoring structural health using a probabilistic measure," *Computer-Aided Civil and Infrastructure Engineering*, vol. 16, no. 1, pp. 1–11, 2001.

[37] H. F. Lam, J. H. Yang, Q. Hu, and C. T. Ng, "Railway ballast damage detection by Markov chain Monte Carlo-based Bayesian method," *Structural Health Monitoring*, vol. 17, no. 3, pp. 706–724, 2018.

[38] J. Wang, X. Z. Liu, and Y. Q. Ni, "A Bayesian probabilistic approach for acoustic emission-based rail condition assessment," *Computer-Aided Civil and Infrastructure Engineering*, vol. 33, no. 1, pp. 21–34, 2018.

[39] S. C. Kuok and K. V. Yuen, "Bayesian nonparametric modeling of structural health indicators under severe typhoons and its application to modeling modal frequency," *Journal of Aerospace Engineering*, vol. 32, no. 4, Article ID 04019036, 2019.

[40] J. L. Beck and S. K. Au, "Bayesian updating of structural models and reliability using Markov chain Monte Carlo simulation," *Journal of Engineering Mechanics*, vol. 128, no. 4, pp. 380–391, 2002.

[41] Y. Garbatov and C. G. Soares, "Bayesian updating in the reliability assessment of maintained floating structures," *Journal of Offshore Mechanics and Arctic Engineering*, vol. 124, no. 3, pp. 139–145, 2002.

[42] A. Der Kiureghian, "Analysis of structural reliability under parameter uncertainties," *Probabilistic Engineering Mechanics*, vol. 23, no. 4, pp. 351–358, 2008.

[43] A. Strauss, D. M. Frangopol, and S. Kim, "Use of monitoring extreme data for the performance prediction of structures: Bayesian updating," *Engineering Structures*, vol. 30, no. 12, pp. 3654–3666, 2008.

[44] Y. Q. Ni, Y. W. Wang, and C. Zhang, "A Bayesian approach for condition assessment and damage alarm of bridge expansion joints using long-term structural health monitoring data," *Engineering Structures*, vol. 212, Article ID 110520, 2020.

[45] E. Figueiredo, L. Radu, K. Worden, and C. R. Farrar, "A Bayesian approach based on a Markov chain Monte Carlo method for damage detection under unknown sources of variability," *Engineering Structures*, vol. 80, pp. 1–10, 2014.

[46] Y. Q. Ni and R. Chen, "Strain monitoring based bridge reliability assessment using parametric Bayesian mixture model," *Engineering Structures*, vol. 226, Article ID 111406, 2021.

[47] P. Orbanz and Y. W. Teh, "Bayesian nonparametric models," in *Encyclopedia of Machine Learning*, C. Sammut and G. I. Webb, Eds., Springer, Boston, MA, USA, 2010.

[48] S. J. Gershman and D. M. Blei, "A tutorial on Bayesian nonparametric models," *Journal of Mathematical Psychology*, vol. 56, no. 1, pp. 1–12, 2012.

[49] Z. Ghahramani, "Bayesian non-parametrics and the probabilistic approach to modelling," *Philosophical Transactions of the Royal Society A: Mathematical, Physical & Engineering Sciences*, vol. 371, Article ID 20110553, 2013.

[50] D. Chakraborty, N. Kovvali, A. Papandreou-Suppappola, and A. Chattopadhyay, "An adaptive learning damage estimation method for structural health monitoring," *Journal of Intelligent Material Systems and Structures*, vol. 26, no. 2, pp. 125–143, 2015.

[51] T. J. Rogers, K. Worden, R. Fuentes, N. Dervilis, U. T. Tygesen, and E. J. Cross, "A Bayesian non-parametric clustering approach for semi-supervised structural health monitoring," *Mechanical Systems and Signal Processing*, vol. 119, pp. 100–119, 2019.

[52] P. Cheema, M. M. Alamdari, G. A. Vio, F. L. Zhang, and C. W. Kim, "Infinite mixture models for operational modal analysis: an automated and principled approach," *Journal of Sound and Vibration*, vol. 491, Article ID 115757, 2021.
[53] C. E. Rasmussen, "The infinite Gaussian mixture model," in *Advances in Neural Information Processing Systems*, S. A. Solla, T. K. Leen, and K. R. Muller, Eds., MIT Press, Cambridge, MA, USA, 2000.
[54] Y. W. Teh, "Dirichlet process," in *Encyclopedia of Machine Learning*, C. Sammut and G. I. Webb, Eds., Springer, Boston, MA, USA, 2011.
[55] D. J. Aldous, *Exchangeability and Related Topics*, Springer, Berlin, Germany, 1985.
[56] J. Sethuraman, "A constructive definition of Dirichlet priors," *Statistica Sinica*, vol. 4, pp. 639–650, 1994.
[57] R. M. Neal, "Markov chain sampling methods for Dirichlet process mixture models," *Journal of Computational & Graphical Statistics*, vol. 9, no. 2, pp. 249–265, 2000.
[58] K. P. Murphy, *Machine Learning: A Probabilistic Perspective*, MIT Press, Cambridge, MA, USA, 2012.
[59] S. P. Brooks and P. Giudici, "Markov chain Monte Carlo convergence assessment via two-way analysis of variance," *Journal of Computational & Graphical Statistics*, vol. 9, no. 2, pp. 266–285, 2000.
[60] Y. Q. Ni, H. W. Xia, K. Y. Wong, and J. M. Ko, "In-service condition assessment of bridge deck using long-term monitoring data of strain response," *Journal of Bridge Engineering*, vol. 17, no. 6, pp. 876–885, 2012a.
[61] X. Wang, Y. Q. Ni, and K. C. Lin, "Comparison of statistical counting methods in SHM-based reliability assessment of bridges," *Journal of Civil Structural Health Monitoring*, vol. 5, no. 3, pp. 275–286, 2015.
[62] K. Y. Wong, "Stress and traffic loads monitoring of tsing Ma bridge," in *Proceedings of the China Bridge Congress 2007*, Chongqing, China, 2007.
[63] S. Chatterjee, *The Design of Modern Steel Bridges*, Blackwell Science, Hoboken, NJ, USA, 2008.
[64] R. Chen, *Parametric and nonparametric bayesian mixture models for bridge condition assessment*, Ph.D. thesis, The Hong Kong Polytechnic University, Hong Kong, 2020.
[65] D. M. Frangopol, J. S. Kong, and E. S. Gharaibeh, "Reliability-based life-cycle management of highway bridges," *Journal of Computing in Civil Engineering*, vol. 15, no. 1, pp. 27–34, 2001.